

¹ Drought, vegetation productivity, and land cover change in Chile

² Francisco Zambrano^{a,1,*}, Anton Vrielink^b, Francisco Fernández^c, Francisco Meza, Alejandro
³ Venegas-González, Iongel Duran-Llacer, Nicolas Raab, Dylan Craven

^a Universidad Mayor, Hémera Centro de Observación de la Tierra, Facultad de Ciencias, Escuela de Ingeniería en Medio Ambiente y Sustentabilidad, Santiago, Chile, 7500994

^b University of Twente, Faculty of Geo-Information Science and Earth Observation (ITC), Enschede, The Netherlands,

^c Universidad San Sebastian,

⁴ **Abstract**

Central Chile has been the focus of research studies due to the persistent decrease in water supply, which is impacting the hydrological system and vegetation development. This persistent period of water scarcity has been defined as a megadrought. Our objective is to assess the impact of drought on LULCC (land use land cover change) over continental Chile using drought indices of water supply and demand, soil moisture, and their impact on vegetation productivity. The monthly ERA5-Land (ERA5L) variables for precipitation, temperature, and soil moisture were used. From 2001 to 2022, we used the land cover MODIS product MCD12Q1, and from 2000 to 2023, we used the NDVI (Normalized Difference Vegetation Index) product MOD13A3 collection 6.1. As drought indices, we compute the standardized anomaly of cumulative NDVI (zcNDVI), the Standardized Precipitation Evapotranspiration Index (SPEI), the Evaporative Demand Drought Index (EDDI), and the Standardized Soil Moisture Index (SSI). These indices were calculated for time scales of 1, 3, 6, 12, 24, and 36 months, except for zcNDVI, which was for 6 months. We analyze the trend for LULCC, vegetation productivity, and drought indices. Also, we analyzed the temporal correlation of SPI, SPEI, EDDI, and SSI with zcNDVI to gain insights into the impact of water supply and demand on vegetation productivity. Our results showed that LULCC was highest in “Centro,” “Sur,” and “Austral,” with 36%, 31%, and 34% of change in the surface type, respectively. The EDDI shows that water demand has increased for all zones, with a major increase in “Norte Grande.” The drought indices of water supply and soil moisture evidence a decreasing trend, which decreases at longer time scales, from “Norte Grande” to “Sur.” “Austral” is the only zone that shows an increase in supply. Vegetation productivity measures by zcNDVI present a negative trend in “Norte Chico” and “Centro.” On the other hand, forests seem to be the most resistant to drought. The types that show to be most affected by variation in climate conditions are shrublands, savannas, and croplands. The drought indices that have the capability of explaining to a major degree the variance in vegetation productivity are SSI-12, followed by SPEI-24 and SPEI-12 in “Norte Chico” and “Centro.” The results indicate that “Norte Chico” and “Zona Central” are the most sensitive regions to water supply deficits lasting longer than a year. Our results can help develop a robust vegetation productivity forecasting model for land cover classes in Chile.

⁵ **Keywords:** drought, land cover change, satellite

*Corresponding author

Email addresses: francisco.zambrano@umayor.cl (Francisco Zambrano), a.vrielink@utwente.nl (Anton Vrielink), a.vrielink@utwente.nl (Francisco Fernández)

¹This is the first author footnote.

6 **1. Introduction**

7 Drought is often classified as meteorological when there is a decrease in precipitation below the mean
8 average of several years (more than 30 years), hydrological when these anomalies last for long periods (months
9 to years) and affect water systems, and agricultural when the deficit impacts plant health anomalies and
10 leads to decreased productivity (Wilhite and Glantz, 1985). However, it is important to note that drought
11 is also influenced by human activities, which were not considered in the definitions. Thus, Van Loon et al.
12 (2016) and AghaKouchak et al. (2021) have given an updated definition of drought for the Anthropocene,
13 suggesting that it should be considered the feedback of humans' decisions and activities that drives the
14 anthropogenic drought. Simultaneously, drought leads to heightened tree mortality and induces alterations
15 in land cover and land use, ultimately affecting ecosystems (Crausbay et al., 2017). Even though many
16 ecological studies have misinterpreted how to characterize drought, for example, sometimes considering
17 "dry" conditions as "drought" (Slette et al., 2019). Then, Crausbay et al. (2017) proposed the ecological
18 drought definition as "an episodic deficit in water availability that drives ecosystems beyond thresholds of
19 vulnerability, impacts ecosystem services, and triggers feedback in natural and/or human systems." In light
20 of current global warming, it is crucial to study the interaction between drought and ecosystems in order to
21 understand their feedback and impact on water security. (Bakker, 2012)

22 Human-induced greenhouse gas emissions have increased the frequency and/or intensity of drought as a
23 result of global warming, according to the sixth assessment report (AR6) of the Intergovernmental Panel
24 on Climate Change (IPCC) (Calvin et al., 2023). The evidence supporting this claim has been strength-
25 ened since AR5 (IPCC, 2013). Recent studies, however, have produced contrasting findings, suggesting
26 that drought has not exhibited a significant trend over the past forty years. (Vicente-Serrano et al., 2022;
27 Kogan et al., 2020). Vicente-Serrano et al. (2022) analyzed the meteorological drought trend on a global
28 scale, finding that only in a few regions has there been an increase in the severity of drought. Moreover,
29 they attribute the increase in droughts over the past forty years solely to an increase in atmospheric evap-
30 orative demand (AED), which in turn enhances vegetation water demand, with important implications for
31 agricultural and ecological droughts. Also, they state that "the increase in hydrological droughts has been
32 primarily observed in regions with high water demand and land cover change". Similarly, Kogan et al. (2020)
33 analyzed the drought trend using vegetation health methods, finding that for the globe, hemispheres, and
34 main grain-producing countries, drought has not expanded or intensified for the last 38 years. Further,
35 the Masson-Delmotte (2021) suggests that there is a high degree of confidence that rising temperatures
36 will increase the extent, frequency, and severity of droughts. Also, AR6 (Calvin et al., 2023) predicts that
37 many regions of the world will experience more severe agricultural and ecological droughts even if global
38 warming stabilizes at 1.5°–2°C. To better evaluate the impact of drought trends on ecosystems, assessments
39 are needed that relate meteorological and soil moisture variables to their effects on vegetation.

40 From 1960 to 2019, land use change has impacted around one-third of the Earth's surface, which is four
41 times more than previously thought (Winkler et al., 2021). Multiple studies aim to analyze and forecast
42 changes in land cover globally (Winkler et al., 2021; Song et al., 2018) and regionally (Chamling and Bera,
43 2020; Homer et al., 2020; Yang and Huang, 2021). Some others seek to analyze the impact of land cover
44 change on climate conditions such as temperature and precipitation (Luyssaert et al., 2014; Pitman et al.,
45 2012). There is less research on the interaction between drought and land cover change (Chen et al., 2022;
46 Akinyemi, 2021; Peng et al., 2017). Peng et al. (2017) conducted a worldwide investigation utilizing net
47 primary production to examine the spatial and temporal variations in vegetation productivity at global
48 level. The study aimed to assess the influence of drought by comparing the twelve-month Standardized
49 Precipitation Evapotranspiration Index (SPEI) and land cover change. According to their findings, drought
50 is responsible for 37% of the decline in vegetation productivity, while water availability accounts for 55% of
51 the variation. Chen et al. (2022) studied the trend of vegetation greenness and productivity and its relation
52 to meteorological drought (SPEI of twelve months in December) and soil moisture at the global level. The
53 results showed lower correlations (<0.2) for both variables. Akinyemi (2021) evaluates drought trends and
54 land cover change using vegetation indices in Botswana in a semi-arid climate. These studies mostly looked
55 at how changes in land cover and vegetation productivity are related to a single drought index (SPEI) over

56 a single time period of 12 months. SPEI takes into account the combined effect of precipitation and AED as
57 a water balance, but it does not allow us to know the contribution of each variable on its own. Some things
58 worth investigating in terms of land cover change and vegetation productivity are: i) How do they respond
59 to short- to long-term meteorological droughts? ii) How do they behave in humid and arid climatic zones
60 regarding drought? And iii) What is the role of soil moisture? Likewise, there is a lack of understanding of
61 how the alteration in water supply and demand is affecting land cover transformations.

62 Chile's diverse climatic and ecosystem types ([Beck et al. \(2023\)](#); [Luebert and Pliscoff \(2022\)](#)) make it an
63 ideal natural laboratory for studying climate and ecosystems. Additionally, the country has experienced
64 severe drought conditions that have had significant effects on vegetation and water storage. Central Chile
65 faced a persistent precipitation deficit between 2010 and 2022, defined as a megadrought ([Garreaud et al.,](#)
66 [2017](#)), which has impacted the Chilean ecosystem. This megadrought was defined by the Standardized
67 Precipitation Index (SPI) of twelve months in December having values below one standard deviation. Some
68 studies have addressed how this drought affects single ecosystems in terms of forest development ([Miranda](#)
69 [et al., 2020](#); [Venegas-González et al., 2018](#)), forest fire occurrence ([Urrutia-Jalabert et al., 2018](#)), and crop
70 productivity ([Zambrano, 2023](#); [Zambrano et al., 2018, 2016](#)). We found one study regarding land cover and
71 drought in Chile. The study by [Fuentes et al. \(2021\)](#) evaluates water scarcity and land cover change in Chile
72 between 29° and 39° of south latitude. [Fuentes et al. \(2021\)](#) used the SPEI of one month for evaluating
73 drought, which led to misleading results. For example, they did not find a temporal trend in the SPEI but
74 found a decreasing trend in water availability and an increase trend on AED, which in turn should have been
75 capable of being captured with longer time scales of the SPEI. The term "megadrought" in Chile is used to
76 describe a prolonged water shortage that lasts for several years, resulting in a permanent deficit that impacts
77 the hydrological system ([Boisier et al., 2018](#)). Hence, it is imperative to assess temporal scales that take into
78 account the cumulative effect within some years. There is little knowledge about the relationship between
79 drought and ecosystem in Chile; thus, it is important to understand in more detail how meteorological and
80 soil moisture droughts influence ecosystem dynamics to inform adaptation options.

81 A detailed spatiotemporal assessment of the interaction of drought for short- to long-term and land cover
82 change requires information on vegetation as well as weather variables such as precipitation, temperature,
83 and soil moisture. Weather networks in Chile present some disadvantages, such as spatio-temporal gaps, a
84 short history, and irregular quality, which make them difficult to represent the whole extent of the country
85 spatially. In order to do this, we use reanalysis data from ERA5-Land ([Muñoz-Sabater et al., 2021](#)) to create
86 drought indices that consider AED, precipitation, and soil moisture over a range of time periods, from the
87 short to the long term. Also, we use vegetation spectral information and annual land cover change from
88 the Moderate-Resolution Imaging Spectroradiometer (MODIS). We expect to gain insight regarding the
89 temporal evolution of water demand, water supply, and soil moisture, as well as the interaction with land
90 cover change and vegetation productivity. Here, we analyze the multi-dimensional impacts of drought across
91 ecosystems in continental Chile. More specifically, we aim to assess: i) temporal changes in land-use cover
92 and the direction and magnitude of their relationships with drought indices for water demand and supply,
93 soil moisture, and vegetation productivity; ii) short- to long-term temporal trends in multi-scalar drought
94 indices; and iii) the relationship between vegetation productivity and drought indices for water demand and
95 supply and soil moisture across Chilean ecosystems.

96 2. Study area

97 Continental Chile has a diverse climate conditions with strong gradients from north to south and east
98 to west ([Aceituno et al., 2021](#)) (Figure 1 a), which determines its great ecosystem diversity ([Luebert and](#)
99 [Pliscoff \(2022\)](#)) (Figure 1 c). The Andes Mountains are a main factor in climate latitudinal variation
100 ([Garreaud, 2009](#)). In order to characterize the climate and ecosystem of Chile, we utilize the Köppen-Geiger
101 classification system developed by [Beck et al. \(2023\)](#) and the land cover data derived from the MODIS
102 product for the period of 2001–2022, based on the International Geosphere-Biosphere Programme (IGBP)
103 classification scheme proposed by [Friedl and Sulla-Menashe \(2019\)](#). "Norte Grande" and "Norte Chico"

104 predominate in an arid desert climate with hot (Bwh) and cold (Bwk) temperatures. At the south of “Norte
 105 Chico,” the climate changes to an arid steppe with cold temperatures (Bsk). In these two northern regions,
 106 the land is mostly bare, with a minor surface of vegetation types such as shrubland and grassland. In the
 107 zones “Centro” and the north half of “Sur,” the main climate is Mediterranean, with warm to hot summers
 108 (Csa and Csb). Land cover in “Centro” comprises a significant amount of shrubland and savanna (50%),
 109 grassland (16%), forest (8%), and croplands (5%). An oceanic climate (Cfb) predominates in the south
 110 of “Sur” and the north of “Austral.” Those zones are high in forest and grassland. The southern part of
 111 the country has a tundra climate, and in “Austral”, it is a cold semi-arid area with an extended surface of
 112 grassland, forest, and, to a lesser extent, savanna.

113 3. Materials and Methods

114 3.1. Data

115 3.1.1. Gridded meteorological and vegetation data

116 To analyze the LULCC, we use the IGBP scheme from the MCD12Q1 collection 6.1 from MODIS. This
 117 product has a yearly frequency from 2001 to 2022. The IGBP defines 17 classes; from these, we regrouped
 118 into ten macroclasses, as follows: classes 1-4 to forest, 5-7 to shrublands, 8-9 to savannas, 10 as grasslands,
 119 11 as wetlands, 12 and 14 to croplands, 13 as urban, 15 as snow and ice, 16 as barren, and 17 to water
 120 bodies. Thus, we have a land cover raster time series with the ten classes for 2001 and 2023. Prior to
 121 using this class, we compared it with the types of land cover made by [Zhao et al. \(2016\)](#), which is a more
 122 detailed land cover map of Chile with a 30 m spatial resolution for 2012–2013. It reached a global accuracy
 123 of ~0.82. The procedure of validation is demonstrated in Section S1 of the supplementary material. To derive
 124 a proxy for vegetation productivity, we used the MOD13A3 collection 6.1 product from MODIS ([Didan, 2015](#)). It provides vegetation indices (NDVI and EVI) at 1km of spatial resolution and monthly frequency.
 125 The MOD13A3 and MCD12Q1 were retrieved from the online Data Pool, courtesy of the NASA EOSDIS
 126 Land Processes Distributed Active Archive Center (LP DAAC), USGS Earth Resources Observation and
 127 Science (EROS) Center, Sioux Falls, South Dakota, <https://lpdaac.usgs.gov/tools/data-pool/>.

Table 1: Description of the earth observation data used

Product	Sub-product	Variable	Spatial Resolution	Period	Units	Short Name
ERA5L		Precipitation	0.1°	1981-2023	mm	P
		Maximum temperature			°C	T_{max}
		Minimum temperature			°C	T_{min}
		Volumetric Soil Water Content at 1m			m3/m3	SM
ERA5L*	MOD13A3.061	Atmospheric Evaporative Demand	0.1°	1981-2023	mm	AED
MODIS		Normalized Difference Vegetation Index	1 km	2000-2023		NDVI
MCD12Q1.061		land cover IGBP scheme		2001-2022		land cover

*Derived from ERA5L with Eq. 1.

129 For soil moisture, water supply, and water demand variables, we used ERA5L ([Muñoz-Sabater et al., 2021](#)),
 130 a reanalysis dataset that provides the evolution of the meteorological and soil moisture variables since 1950.
 131 It has a spatial resolution of 0.1° (9 km), hourly frequency, and global coverage. We selected the variables
 132 for total precipitation, maximum and minimum temperature at 2 meters, and volumetric soil water layers
 133 between 0 and 100cm of depth (layer 1 to layer 3).

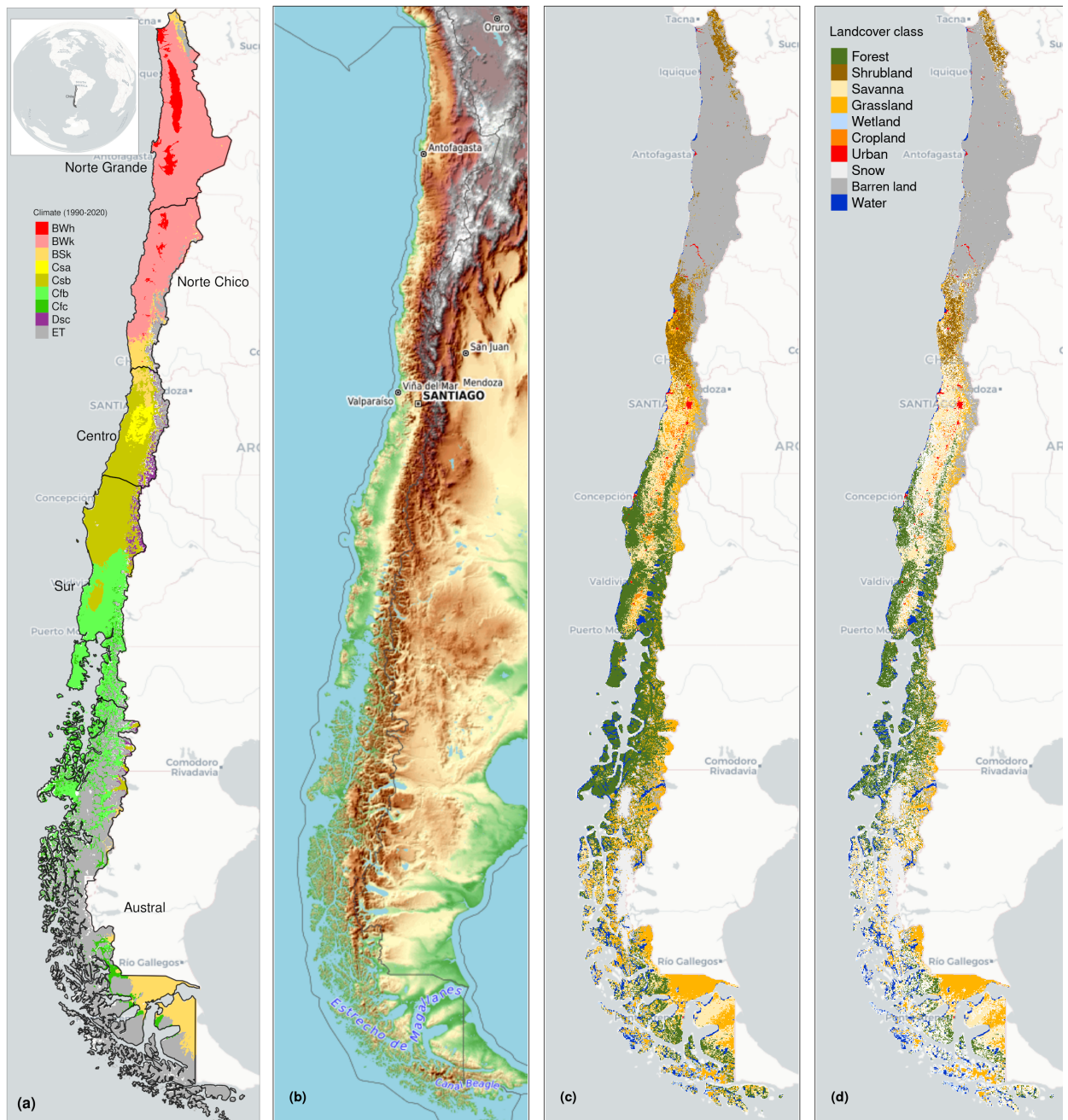


Figure 1: (a) Chile with the Koppen-Geiger climate classes and the five macrozones “Norte Grande”, “Norte Chico”, “Centro”, “Sur”, and “Austral”. (b) Topography reference map. (c) land cover classes for 2022. (d) Persistent land cover classes (> 80%) for 2001-2022

134 3.2. Land cover change and trend

135 To analyze the LULCC, we use the IGBP scheme from the MCD12Q1 collection 6.1 from MODIS. [Zambrano](#)
 136 [et al. \(2018\)](#) and [Fuentes et al. \(2021\)](#) have previously used this product for studies of drought and land
 137 cover. The MCD12Q1 has a yearly frequency from 2001 to 2022. The IGBP defines 17 classes; from these,
 138 we regrouped into ten macroclasses, as follows: classes 1-4 to forest, 5-7 to shrublands, 8-9 to savannas, 10

139 as grasslands, 11 as wetlands, 12 and 14 to croplands, 13 as urban, 15 as snow and ice, 16 as barren, and 17
140 to water bodies. Thus, we have a land cover raster time series with the ten macroclasses for 2001 and 2023.
141 We validate the land cover macroclasses regarding a highly detailed (30 m of spatial resolution) land cover
142 map made for Chile by [Zhao et al. \(2016\)](#) for 2013-2014. Our results showed a global accuracy of ~0.82 and
143 a F1 score of ~0.66. Section S2 in the Supplementary Material shows the procedure for validation.

144 Climate, vegetation development, seasonality, and changes in vegetation type all have an impact on the
145 time series of NDVI. In this study, we want to examine the variation in vegetation productivity across
146 various land cover types and how water demand, water supply, and soil moisture affect it. In order to avoid
147 changes due to a change in the land cover type that will wrongly impact NDVI, we developed a persistence
148 mask for land cover for 2001–2022. Thereby, we reduce an important source of variation on a regional
149 scale. Therefore, we generated a raster mask for IGBP MODIS per pixel using macroclasses that remained
150 unchanged for at least 80% of the years (2001–2022). This enabled us to identify regions where the land
151 cover macroclasses are persistent. We calculated the surface occupied per land cover class into the five
152 macrozones (“Norte Grande” to “Austral”) per year for 2001–2023. After that, we calculated the trend’s
153 change in surface per type. We used the Sen’ slope ([Sen, 1968](#)) based on Mann-Kendall ([Kendall, 1975](#)).

154 *3.3. Trend of drought and land cover change*

155 *3.3.1. Atmospheric Evaporative Demand (AED)*

156 In order to compute the drought indices that uses water demand, it is necessary to first calculate the AED.
157 To do this, we employed the Hargreaves technique ([Hargreaves, 1994](#); [Hargreaves and Samani, 1985](#)), by
158 applying the following equation:

$$AED = 0.0023 \cdot Ra \cdot (T + 17.8) \cdot (T_{max} - T_{min})^{0.5} \quad (1)$$

159 where Ra ($MJ\ m^2\ day^{-1}$) is extraterrestrial radiation; T , T_{max} , and T_{min} are mean, maximum, and
160 minimum temperature ($^{\circ}C$). We calculate the centroid coordinates per pixel and use the latitude to estimate
161 Ra .

162 We chose the method of Hargreaves to estimate AED because of its simplicity, which only requires tem-
163 peratures and extrarrestrial radiation. Also, it has been recommended over other methods (e.g., Penman-
164 Monteith) when the access to climatic variables is limited ([Vicente-Serrano et al., 2014](#)).

165 *3.3.2. Non-parametric calculation of drought indices*

166 To derive the drought indices of water supply and demand, soil moisture, and vegetation we used the ERA5L
167 dataset and the MODIS product, with a monthly frequency for 1981-2023 and 2000-2023, respectively.

168 The drought indices correspond to a historical anomaly with regard to a variable (e.g., meteorological,
169 vegetation, or soil moisture). To account for the anomaly, the common practice is to derive it following
170 a statistical parametric methodology in which it is assumed that the statistical distribution of the data is
171 known ([Heim \(2002\)](#)). A wrong decision is usually the highest source of uncertainty ([Laimighofer and Laaha
\(2022\)](#)). In the case of Chile, due to its high degree of climatic variability, it is complex to choose a proper
172 distribution without previous research. Here, we follow a non-parametric methodology for the calculation
173 of the drought indices, in a similar manner as the framework proposed by [Farahmand and AghaKouchak
\(2015\)](#); [Hobbins et al. \(2016\)](#); [McEvoy et al. \(2016\)](#).

176 For the purpose of monitoring water supply drought, we used the well-known Standardized Precipitation
177 Index (SPI), which the World Meteorological Organization (WMO) recommended. The SPI solely relies on
178 precipitation data. Also, it has been used worldwide for the study of drought, including in Chile ([Garreaud
et al. \(2017\)](#); [Zambrano et al. \(2017\)](#)). The primary cause of drought is precipitation anomalies, and

180 temperature usually makes it worse (Luo et al. 2017). Nowadays, there is an increase in attention toward
 181 using water demand separately to monitor droughts. (Vicente-Serrano et al. (2020); Noguera et al. (2022)).
 182 Thus, to evaluate water demand, we chose the Evaporative Demand Drought Index (EDDI), developed
 183 by Hobbins et al. (016) and McEvoy et al. (2016), which is based on the AED. EDDI is currently used for
 184 monitoring drought in the United States (<https://psl.noaa.gov/eddi/>). In our case, we used only temperature
 185 for AED, a difference from the original formulation of EDDI, which also considered wind besides temperature.
 186 To consider the combined effect of water supply and demand, we selected the SPEI, which corresponds to
 187 a balance between precipitation and AED. Vicente-Serrano et al. (2010) proposed the SPEI, and it has
 188 improved the SPI by incorporating temperature for drought monitoring. For SPEI, an auxiliary variable D
 189 = P -AED is calculated. Soil moisture is the main driver of vegetation productivity, particularly in semi-arid
 190 regions (Li et al. (2022)). Hence, for soil water drought, we used the SSI (Standardized Soil Moisture Index)
 191 (Hao and AghaKouchak 2013; A. AghaKouchak 2014) which is a multi-scale index similar to SPI, SPEI, and
 192 EDDI. In our case, for the SSI, we used the average soil moisture from ERA5L at 1m depth. Finally, for
 193 the proxy of productivity, we used the zcNDVI proposed by Zambrano et al. (2018) which will be derived
 194 from the NDVI retrieved from MOD13A1.

195 To derive the drought indices, first we must calculate the sum of the variables with regard to the time
 196 scale (s). In this case, for generalization purposes, we will use V , referring to variables P , AED , D , $NDVI$,
 197 and SM (#ref{tab-desEOD}). We cumulated each V over the time series of n values (months), and for the
 198 time scales s :

$$A_{si} = \sum_{i=n-s-i+2}^{n-i+1} V_i \quad \forall i \geq n - s + 1 \quad (2)$$

199 The A_{si} corresponds to a moving window (convolution) that sums the variable for time scales s from the
 200 last month, month by month, until the first month in which it could sum for s months. Once the variable
 201 is cumulated over time for the scale s . Thus, the empirically derived probabilities are obtained through an
 202 inverse normal approximation (Abramowitz and Stegun, 1968). Then, we used the empirical Tukey plotting
 203 position (Wilks, 2011) over A_i to derive the $P(A_i)$ probabilities across a period of interest:

$$P(A_i) = \frac{i - 0.33}{n + 0.33} \quad (3)$$

204 The drought indices *SPI*, *SPEI*, *EDDI*, *SSI*, and *zcNDVI* are obtained following the inverse normal
 205 approximation:

$$DI(A_i) = W - \frac{C_0 + C_1 \cdot W + c_2 \cdot W^2}{1 + d_1 \cdot W + d_2 \cdot W^2 + d_3 \cdot W^3} \quad (4)$$

206 DI is referring to the drought index calculated for the variable V . The values for the constants are:
 207 $C_0 = 2.515517$, $C_1 = 0.802853$, $C_2 = 0.010328$, $d_1 = 1.432788$, $d_2 = 0.189269$, and $d_3 = 0.001308$. For
 208 $P(A) \leq 0.5$, $W = \sqrt{-2 \cdot \ln(P(A))}$, and for $P(A_i) > 0.5$, replace $P(A_i)$ with $1 - P(A_i)$ and reverse the sign
 209 of $DI(A_i)$.

210 The drought indices were calculated for time scales of 1, 3, 6, 12, 24, and 36 months at a monthly frequency
 211 for 1981–2023 in order to be used for short- to long-term evaluation of drought. In the case of the proxy of
 212 vegetation productivity (zcNDVI) it was calculated for a time scale of six months at monthly frequency for
 213 2000–2023. For zcNDVI, we test time scales of 1, 3, 6, and 12 months; we choose to use six months because
 214 that shows a more robust representation of vegetation productivity due to the seasonality of vegetation in
 215 Chile.

216 3.3.3. Trend of drought indices

217 To estimate if there are significant positive or negative trends for the drought indices, we used the non-
218 parametric test of Mann-Kendall ([Kendall, 1975](#)). To determine the magnitude of the trend, we used Sen's
219 slope ([Sen, 1968](#)). Some of the advantages of applying this methodology are that the Sen's slope is not
220 affected by outliers as regular regression does, and it is a non-parametric method that is not influenced by
221 the distribution of the data. We applied Mann-Kendall to see if the trend was significant and Sen's slope
222 to estimate the magnitude of the trend. We did this to the six time scales from 1981 to 2023 (monthly
223 frequency) and the indices SPI, EDDI, SPEI, and SSI. Thus, we have trends per index and time scale (24 in
224 total). Then, we extracted the trend aggregated by macrozone and per land cover persistent macroclasses.

225 3.4. Drought impacts on vegetation productivity within land cover

226 We analyzed the trend of vegetation productivity over the unchanged land cover macroclasses. This way,
227 we tried to reduce the noise in the vegetation due to a change in land cover from year to year. To achieve
228 this, we will use the persistent mask of land cover macroclasses, which are the types that remain more than
229 80% of the time for 2001–2022. We used this to evaluate the trend in zcNDVI per land cover class and
230 macrozone.

231 We examine the drought indices of water demand, water supply, soil moisture, and their connection with
232 vegetation productivity to investigate two main questions: i) whether short-term or long-term time scales
233 have a greater impact on vegetation across Chile and its specific regions; and ii) the spatial variation
234 in the strength of the correlation between the variables and time scales. Then, we will summarize for
235 each land cover class and macrozone. Thus, we will be able to advance in understanding how climate
236 is affecting vegetation, considering the impact on the five macroclasses of vegetation: forest, cropland,
237 grassland, savanna, and shrubland.

238 We conducted an analysis on the linear correlation between the indices SPI, SPEI, EDDI, and SSI over
239 time periods of 1, 3, 6, 12, 24, and 36 months, and zcNDVI. The objective is to determine the impact of
240 soil moisture and water demand and supply on vegetation productivity. We used a method similar to that
241 used by [Meroni et al. \(2017\)](#) which compared the SPI with the cumulative FAPAR (Fraction of Absorbed
242 Photosynthetically Active Radiation). A pixel-to-pixel linear correlation analysis was performed for each
243 index within the persistent mask of land cover macroclasses. To begin, the Pearson coefficient of correlation
244 is computed for each of the six time scales. A significant time scale is identified as the one that attains the
245 highest correlation ($p < 0.05$). Subsequently, the Pearson correlation coefficient corresponding to the time
246 scales at which the value peaked was extracted. As a result, for each index, we generated two raster maps:
247 1) containing the raster with values of the time scales that reached the maximum correlation, and 2) having
248 the value of the correlation obtained.

249 3.5. Software and packages used

250 For the downloading, processing, and analysis of the spatio-temporal data, we used the open source software
251 for statistical computing and graphics, R ([R Core Team, 2023](#)). For downloading ERA5L, we used the
252 `{ecmwfr}` package ([Hufkens et al., 2019](#)). For processing raster data, we used `{terra}` ([Hijmans, 2023](#)) and
253 `{stars}` ([Pebesma and Bivand, 2023](#)). For managing vectorial data, we used `{sf}` ([Pebesma, 2018](#)). For the
254 calculation of AED, we used `{SPEI}` ([Beguería and Vicente-Serrano, 2023](#)). For mapping, we use `{tmap}`
255 ([Tennekes, 2018](#)). For data analysis, the suite `{tidyverse}` ([Wickham et al., 2019](#)) was used.

256 4. Results

257 5. Land cover change and trend

258 For vegetation, we obtained and use hereafter five macroclasses of land cover from IGBP MODIS: forest,
259 shrubland, savanna, grassland, and croplands. Figure 1c shows the spatial distribution of the macroclasses

Table 2: Surface of the land cover class that persist during 2001-2022

macrozone	Surface [km ²]						
	Forest	Cropland	Grassland	Savanna	Shrubland	Barren land	
Norte Grande		886		7,910	171,720		
Norte Chico		90	4,283	589	16,321	84,274	
Centro	3,739	1,904	7,584	19,705	844	12,484	
Sur	72,995	1,151	7,198	15,906		2,175	
Austral	60,351		54,297	19,007	249	7,218	
Total	—	137,085	3,145	74,247	55,206	25,324	277,870

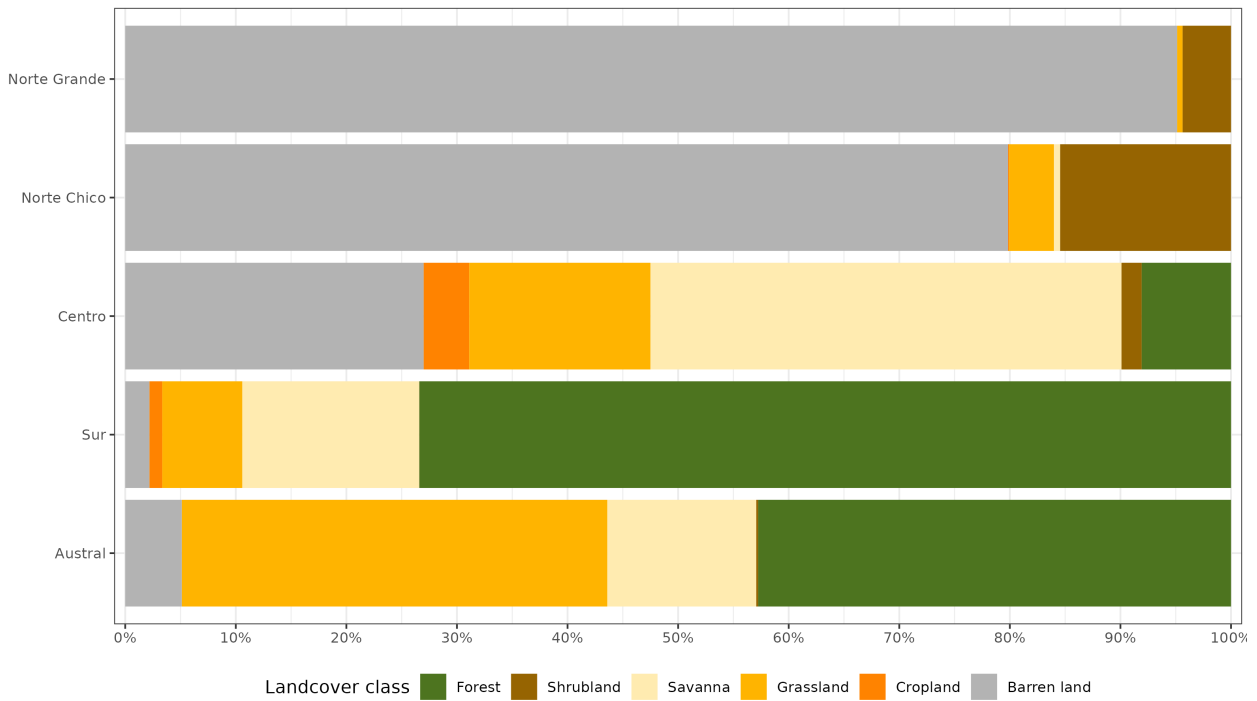


Figure 2: Proportion of land cover class from the persistent land cover for 2001-2022 (>80%) per macrozone

through Chile for the year 2022. Figure 1d shows the macroclasses of land cover persistance (80%) during 2021–2022, respectively (#ref{tab-landcoverSurf}). Within continental Chile, barren land is the land cover class with the highest surface area (277,870 km²). The largest type of vegetation, with 137,085 km², is forest. Grassland (74,247 km²), savanna (55,206 km²), shrubland (25,324 km²), and cropland (3,146 km²) are the other types (Table 2). The macrozones with major changes for 2001–2022 were “Centro,” “Sur,” and “Austral,” with 36%, 31%, and 34% of their surface changing the type of land cover, respectively (Figure 1 and #ref{tab-landcoverTrend}). Figure 2 shows the summary of the proportion of surface per land cover class and macrozone, derived from the persistance mask over continental Chile.

The “Norte Chico” shows an increase in barren land of $111 \text{ km}^2 \text{yr}^{-1}$ and a reduction in the class savanna of $70 \text{ km}^2 \text{yr}^{-1}$. In the “Centro” and “Sur,” there are changes with an important reduction in savanna (136 to $318 \text{ km}^2 \text{yr}^{-1}$), and an increase in shrubland and grassland. Showing a change for more dense vegetation types. It appears to be a shift in the area cultivated (croplands) from the “Centro” to the “Sur.” Also, there is a high increase in forest ($397 \text{ km}^2 \text{yr}^{-1}$) in the “Sur,” replacing the savanna lost (#ref{tab-landcoverTrend}).

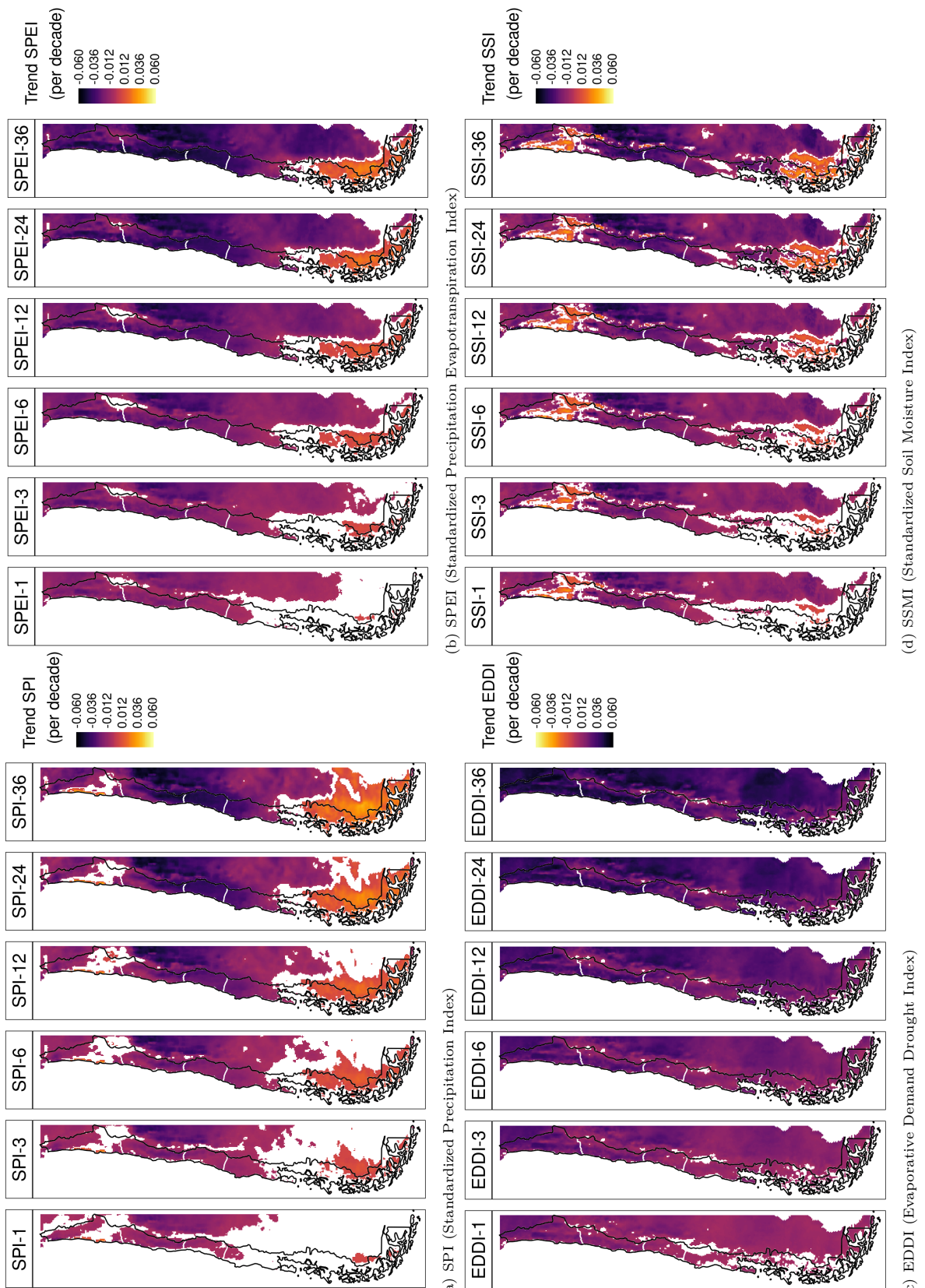
Table 3: The value of Sen’s slope trend next to the time-series plot of surface per land cover class (IGBP MCD12Q1.016) for 2001–2022 through Central Chile. Values of zero indicate that there was not a significant trend. Red dots on the plots indicate the maximum and minimum values of surface.

macrozone	Trend of change [$\text{km}^2 \text{ year}^{-1}$]											
	Forest		Cropland		Grassland		Savanna		Shrubland		Barren land	
	x	y	x	y	x	y	x	y	x	y	x	y
Norte Grande							0.0				0.0	0.0
Norte Chico				-12.1			0.0		-70.0		0.0	111.2
Centro		0.0			-22.4		83.2		-136.2		146.0	22.9
Sur		396.6		37.8		0.0		-318.8				0.0
Austral		0.0			0.0				172.1		-36.9	-93.2

273 5.1. Trend on drought and its relation to land cover change

274 5.1.1. Trend of drought indices

275 Figure 3 shows the spatial variation of the trend for the drought indices from short- to long-term scales.
276 SPI and SPEI have a decreasing trend from “Norte Chico” to “Sur.” However, there is an increasing trend
277 in “Austral.” The degree of the trend is stronger at higher time scales. The SSI indicates that in “Norte
278 Grande,” there are surfaces that have increased in the southwest part and in the northeast have decreased,
279 and is shown for all time scales. Similar to SPI and SPEI, SSI decreases at higher time scales. EDDI showed
280 a positive trend for the whole of continental Chile, with a higher trend toward the north and a descending
281 gradient toward the south. The degree of trend increases at higher time scales.



(c) EDDI (Evaporative Demand Drought Index)

(d) SSMI (Standardized Soil Moisture Index)

Figure 3: Linear trend of the drought index (*) at time scales of 1, 3, 6, 12, 24, and 36 months for 1981-2023

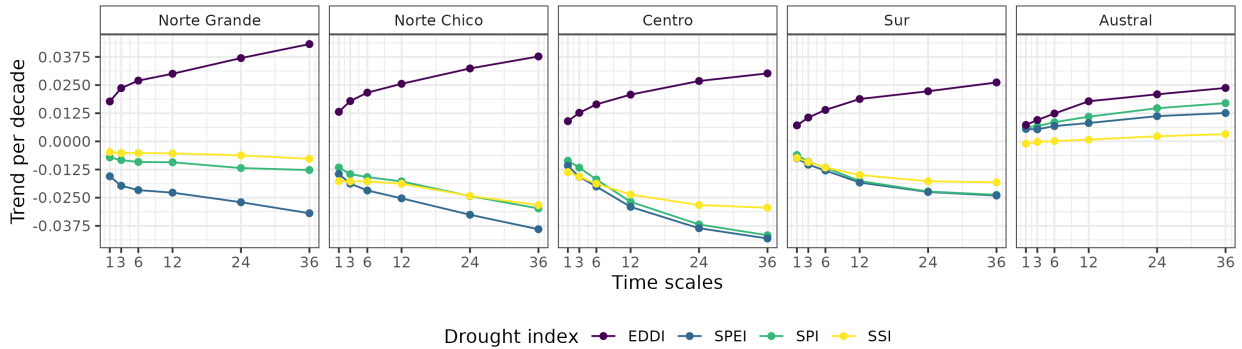


Figure 4: Trend per decade for the drought indices SPI, EDDI, SPEI, and SSI aggregated by macrozone.

In Figure 4, the averaged aggregation per macrozone, drought index, and time scale are shown. The macrozones that have the lowest trend are “Norte Chico” and “Centro,” where the SPI, SPEI, and SSI show that it decreases at longer time scales. Potentially explained due to the prolonged reduction in precipitation that has affected the hydrological system in Chile. At 36 months, it reaches trends between -0.03 and -0.04 (z-score) per decade for SPI, SPEI, and SSI. For “Sur,” the behavior is similar, decreasing at longer scales and having between -0.016 and -0.025 per decade for SPI, SPEI, and SSI. “Norte Grande” has the highest trend at 36 months for EDDI (0.042 per decade), and “Centro” has the lowest for SPI and SPEI. In “Norte Grande” and “Norte Chico,” which are in a semi-arid climate, it is evident that the EDDI has an effect on the difference between the SPI and SPEI index, which is not seen in the other macrozones. Contrary to the other macrozones, “Austral” showed an increase in all indices, being the highest for EDDI at 36 months (0.025) and the lowest for SSI, which shows only a minor increase in the trend.

5.1.2. Relationship between drought indices and land cover change

We look at the relationship between drought index and land cover change in Figure 5 by comparing the trends in land cover change (in terms of the total surface area per land cover type and macrozone) and drought indexes. Figure 5 shows that the negative trends in cropland (-0.029) and savanna (-0.026) in “Norte Chico” are the highest and are associated with an increase trend in EDDI and a decreasing trend in SPI, SPEI, and SSI. On the contrary, the shrubland in “Centro” has an increase (0.04) linked to a decrease in SPI, SPEI, and SSI and to an increase in EDDI. In “Austral,” the positive trend in shrubland fits with the positive trend in all the drought indices. The rest of the land cover types in the macrozones show weak associations with water supply, water demand, or soil moisture drought indices.

5.2. Drought impacts on vegetation productivity within land cover

5.2.1. Vegetation productivity

In Figure 6 it is showed the spatial map of trends in zcNDVI ([fig-zcNDVI_var]a) and the temporal variation of zcNDVI within the aggregated macrozones ([fig-zcNDVI_var]b). In “Norte Grande,” vegetation productivity, as per the z-index, exhibits a yearly increase of 0.02 with respect to grassland and shrubland categories. There is a negative trend in “Norte Chico” with -0.04 and “Centro” with -0.02 per decade. In the “Norte Chico,” savanna (-0.05) has the lowest trend, and the rest of the types are around -0.04. In “Centro,” shrubland reaches -0.06, grassland -0.05, and croplands and savanna -0.01 per decade. This could be associated either with a reduction in vegetation surface, a decrease in biomass, or browning ([Miranda et al., 2023](#)). Vegetation reached its lowest values since the year 2019, with an extreme condition in early 2020 and 2022 in the “Norte Chico” and “Centro”. The “Sur” and “Austral” show a positive trend of around 0.016 per decade (Figure 6). Despite the croplands suffering from drought just as badly as the

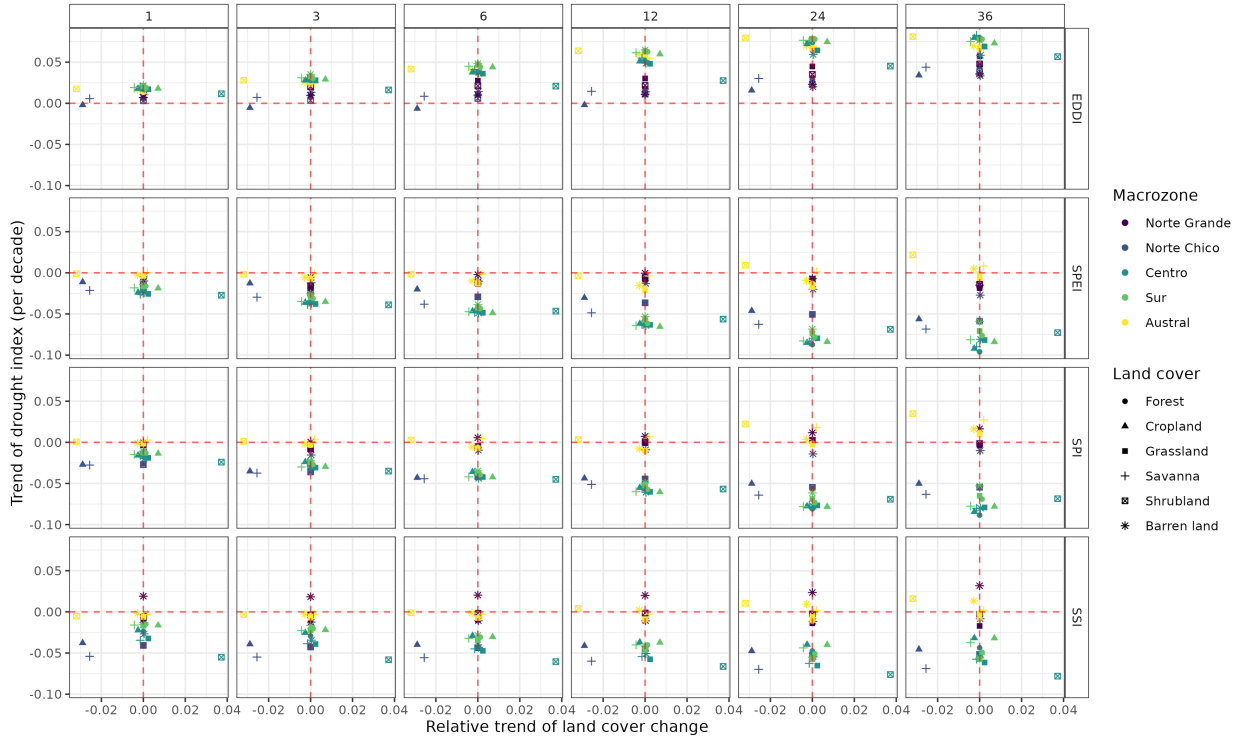


Figure 5: Relationship between the trend in land cover change and the trend in drought indices for the five macrozones. Vertical panels correspond to 1, 3, 6, 12, 24, and 36 months of the time scale by drought index. Horizontal panels show each drought index

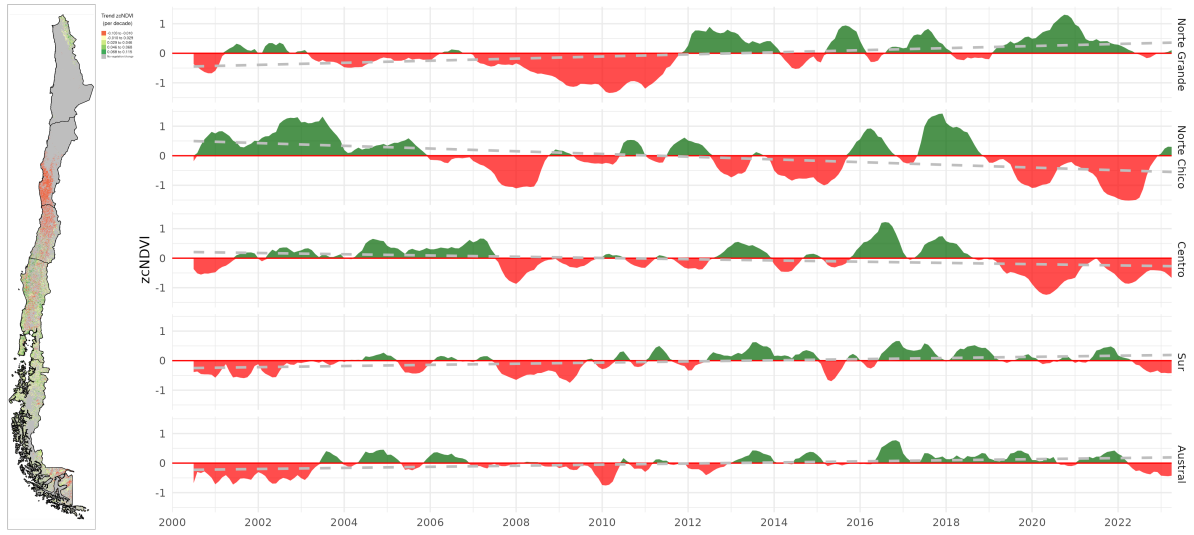


Figure 6: (a) Map of the linear trend of the index zcNDVI-6 for 2001–2023. Greener colors indicate a positive trend; redder colors correspond to a negative trend and a decrease in vegetation productivity. Grey colors indicate either no vegetation or a change in land cover type for 2001–2022. (b) Temporal variation of zcNDVI-6 aggregated at macrozone level within continental Chile. Each horizontal panel corresponds to a macrozone from ‘Norte Grande’ to ‘Austral’.

native vegetation in “Norte Chico,” the savanna and shrubland appears to be the region most affected by a
 negative trend in vegetation productivity.

316 5.2.2. Correlation between vegetation productivity and drought indices

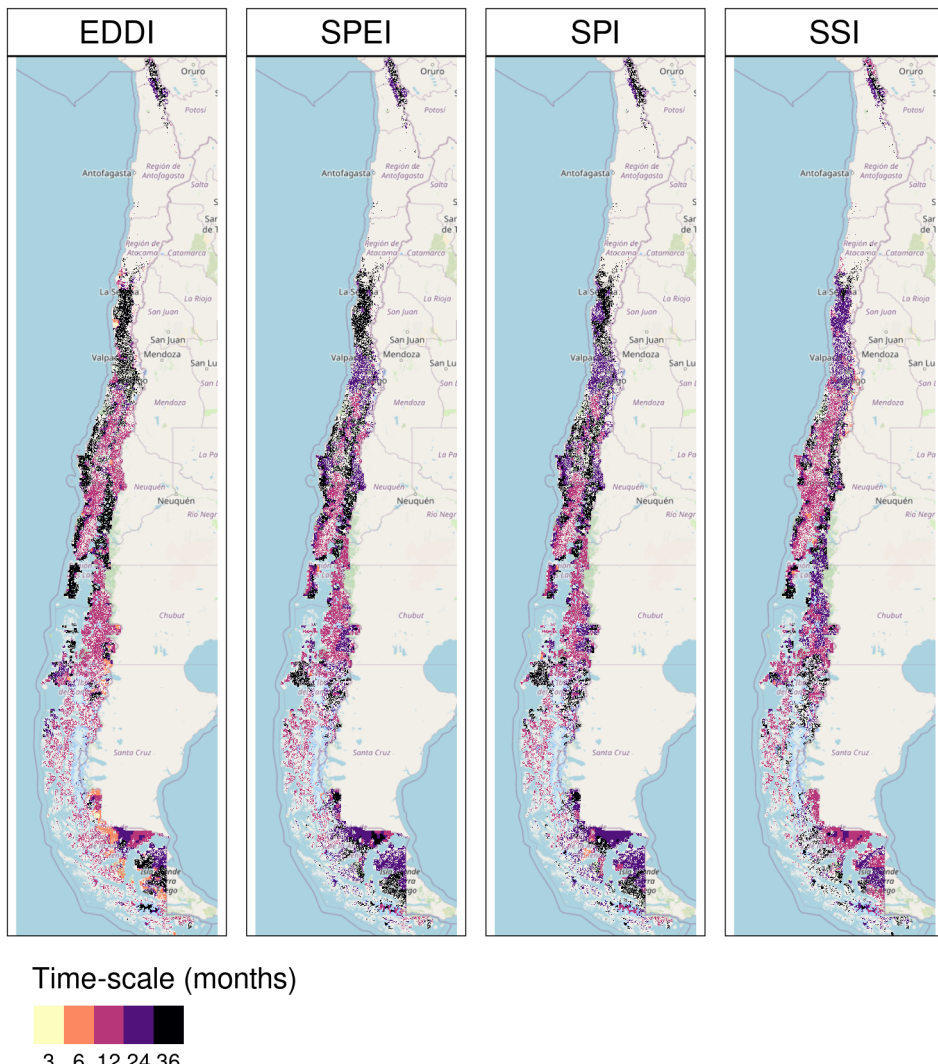


Figure 7: Time scales per drought index that reach the maximum coefficient of determination

317 Figure 7 is a map that shows the highest coefficient of determination (r^2 , or rsq) found in the
 318 regression analysis between different drought indicators and plant productivity over time. The spatial
 319 variation of time scales reached per index is mostly for time scales above 12 months. In the case of SSI,
 320 the predominant scales are 6 and 12 months. For all indices, to the north, the time scales are higher and
 321 diminish toward the south until the south part of “Austral” increases. In Figure 8, the map of Pearson
 322 correlation values is shown. The EDDI reached correlations above 0.5 between “Norte Chico” and “Sur.”
 323 The correlation changes from negative to positive toward the Andes Mountains and to the sea, just as in
 324 the northern part of “Austral.” The SPI and SPEI have similar results, with the higher values in “Norte
 325 Chico” and “Centro” being higher than 0.6. Following a similar spatial pattern as EDDI. The SSI showed
 326 to be the index that has a major spatial extension with a higher correlation. It has a similar correlation to
 327 SPI and SPEI for “Norte Chico” and “Sur,” but has improvements for “Sur.”

328 In #ref{tab-corlandcover}, we aggregate per macrozone and landcover the correlation analysis presented
 329 in Figure 7 and Figure 8. According to what is shown, forests seem to be the most resistant to drought.

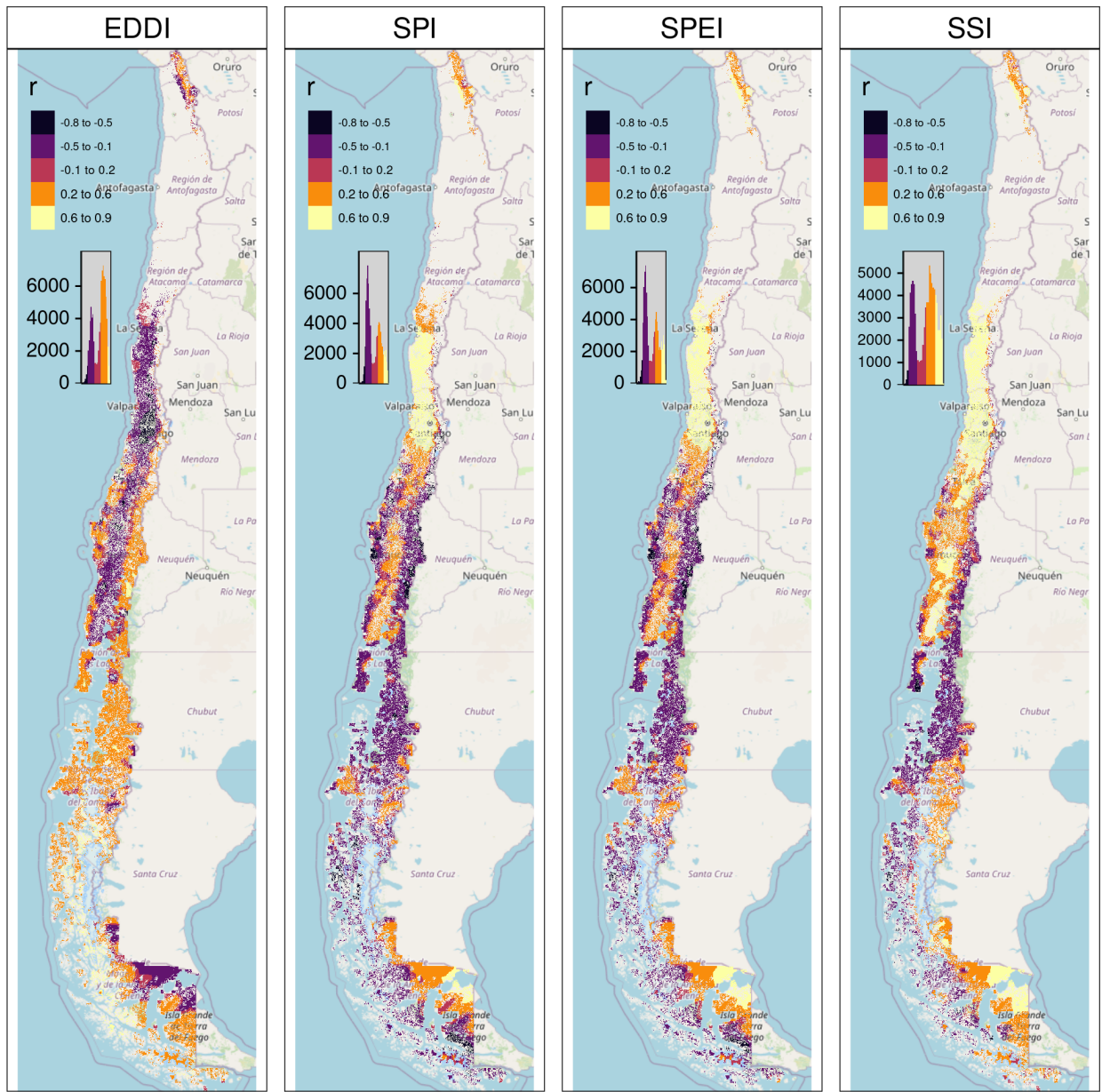


Figure 8: Pearson correlation value for the time scales and drought index that reach the maximum coefficient of determination

330 Showing that only “Centro” is slightly ($rsq = 0.25$) impacted by a 12-month soil moisture deficit (SSI-12).
 331 In the “Norte Chico” and to a lesser extent in the “Norte Grande,” it is evident that a SSI-12 with a $rsq = 0.45$ and a decrease in water supply (SPI-36 and SPEI-24 with $rsq = 0.28$ and 0.34, respectively) have
 332 an impact on grasslands. However, this type was unaffected by soil moisture, water supply, or demand in
 333 macrozones further south. The types that show to be most affected by variation in climate conditions are
 334 shrublands, savannas, and croplands. For savannas in “Norte Chico,” the SSI-12 and SPI-24 reached an
 335 rsq of 0.74 and 0.58, respectively. This value decreases to the south, but the SSI-12 is still the variable
 336 explaining more of the variation in vegetation productivity ($rsq = 0.45$ in “Centro” and 0.2 in “Sur”). In
 337 the case of croplands, the SPEI-12, SPI-36, and SSI-12 explain between 45% and 66% of the variability in
 338

Table 4: Summary per land cover macroclass and macrozone regarding the correlation between zcNDVI with the drought indices EDDI, SPI, SPEI, and SSI for time scales of 1, 3, 6, 12, 24, and 36. The numbers in each cell indicate the time scale that reached the maximum correlation for the land cover and macrozone, and the color indicates the strength of the r-squared obtained with the index and the time scale.

macrozone	Forest				Cropland				Grassland				Savanna				Shrubland			
	EDDI	SPI	SPEI	SSI	EDDI	SPI	SPEI	SSI	EDDI	SPI	SPEI	SSI	EDDI	SPI	SPEI	SSI	EDDI	SPI	SPEI	SSI
Norte Grande									36	36	36	12								
Norte Chico					36	36	12	12	36	36	24	12	36	24	24	12	36	36	24	12
Centro	36	36	12	6	12	12	6	6	12	12	12	36	12	12	12	36	24	24	12	
Sur	36					6	6	6	6	6	6	12	6	6	6	6				
Austral	6	6									6	12	12	6	6	12				
<p>r-squared 0.2 0.4 0.6</p>																				

339 “Norte Chico.” The type of land most impacted by climatic variation was shrubland, where soil moisture
 340 explained 59% and precipitation, 37%, in “Norte Chico” and “Centro,” with SSI-12 being the most relevant
 341 variable, then SPI-36 in “Norte Chico” and SPI-24 in “Sur.”

342 6. Discussion

343 6.1. Drought trend and attribution to land cover

344 Vicente-Serrano et al. (2022), in a study at the global scale of drought trends, indicate that there have not
 345 been significant trends in meteorological drought since 1950. Also, state that the increase in hidrological
 346 trend in some parts of the globe (northeast Brazil and the Mediterranean region) is related to changes
 347 in land cover and specifically to the rapidly increasing irrigated area, which consequently increases water
 348 extraction. Kogan et al. (2020) analyzed the agricultural drought impact globally and in the main grain
 349 producer countries, finding that “since 1980, the Earth warming has not changed the drought area or
 350 intensity.” In our study, we considered the variation in vegetation productivity in Chile for areas without
 351 changes in land cover, to avoid misleading conclusions that could be related to the increase in water demand
 352 due to land cover change. Our results show a contrasting perspective. There has been a significant trend
 353 in the decline of vegetation productivity (zcNDVI) since 2000 for “Norte Chico” and “Centro,” which has
 354 been extreme between 2020 and 2022, seemly due to an intense hydrological drought due to the persistance
 355 of the mega drought (Garreaud et al., 2017). However, a rise in irrigated land doesn’t seem to have an
 356 impact on this hydrological drought. Despite using the persistance mask for vegetation’s trend analysis,
 357 cropland, which is the most water-demand type, showed a decrease trend in “Norte Chico” and “Centro.”
 358 Also, there was an increase in barren land for both types. These changes are associated with a decrease
 359 in water demand from vegetation. Nonetheless, we used the persistant land cover to ensure that the pixel
 360 has the same class; in the case of croplands, it could happen that some areas had changed crops for others
 361 with higher water consumption and consequently increase water demand. But this effect should be minor
 362 compared to the results from land cover change at this scale of analysis.

363 On the other hand, for “Norte Chico” and “Centro,” our results show a decrease in trends of water supply
 364 (SPI and SSI), which are higher at larger time scales, which is evidence of the hydrological drought. We say
 365 that what happened in central Chile goes against what has been found on a global scale (Vicente-Serrano
 366 et al., 2022; Kogan et al., 2020). This shows that the main cause of the hydrological drought in Chile was
 367 a steady drop in water supply made worse by an increase in AED, but it seems that in zones most affected

368 by drought, the main cause is not an increase in water demand by vegetation like irrigated crops. Finally,
369 north-central Chile has experienced a decline in vegetation productivity across all macroclasses, which is
370 primarily attributable to variations in water supply and soil moisture. An increase in water demand, such
371 as an increase in the surface area of irrigated crops, could strengthen this trend.

372 *6.2. Land cover types and their impact by drought*

373 We discovered that croplands, savannas, and shrubland are the most susceptible to climatic changes and are
374 most affected by the 12-month soil moisture deficit. In a study in the Yangtze River Basin in China, [Jiang et al. \(2020\)](#) analyzed the impact of drought on vegetation using the SPEI and the Enhanced Vegetation
375 Index (EVI). They found that cropland was more sensitive to drought than grassland, showing that cropland
377 responds strongly to short- and medium-term drought (< SPEI-6). In our case, the SPEI-12 was the one that
378 most impacted the croplands in “Norte Chico” and “Centro.” In general, most studies show that croplands
379 are most sensitive to short-term drought (< SPI-6) ([Zambrano et al., 2016](#); [Potopová et al., 2015](#); [Dai et al., 2020](#);
380 [Rhee et al., 2010](#)). Short-term precipitation deficits impact soil water, and thus less water is available
381 for plant growth. However, we found that in “Norte Chico,” an SPI-36 and SPEI-12 had a higher impact,
382 which are associated with hydrological drought (long-term), and in “Centro,” an SPI-12 and SPEI-12. Thus,
383 we attribute this impact to the hydrological drought that has decreased groundwater storage ([Taucare et al., 2024](#)),
384 which in turn is impacted by long-term deficits, and consequently, the vegetation is more dependent on
385 groundwater. In “Sur” and “Austral,” the correlations between drought indices and vegetation productivity
386 decrease, as do the time scales that reach the maximum r-squared. What can be explained is that, south of
387 “Centro,” predominate forest and grassland, the most resistant types. Also, drought episodes have been less
388 frequent and intense. The drought episodes have had a lower impact on water availability for vegetation.

389 According to [Senf et al. \(2020\)](#), severe drought conditions in Europe are a significant cause of tree mortality.
390 However, we found that forest is the type of land cover macroclass less affected by variation in drought indices,
391 being the most resistant land cover class to drought. Supporting this is [Fathi-Taperasht et al. \(2022\)](#), who
392 assert that Indian forests are the most drought-resistant and recover rapidly. Similarly, the work of [Wu et al. \(2024\)](#), who analyzed vegetation loss and recovery in response to meteorological drought in the humid
393 subtropical Pearl River basin in China, indicates that forests showed higher drought resistance. Using
395 Vegetation Optical Depth (VOD), kNDVI, and EVI, [Xiao et al. \(2023\)](#) test the resistance of ecosystems
396 and find that ecosystems with more forests are better able to handle severe droughts than croplands. They
397 attribute the difference to a deeper rooting depth of trees, a higher water storage capacity, and different
398 water use strategies between forest and cropland ([Xiao et al., 2023](#)).

399 In contrast to what we obtained, [Venegas-González et al. \(2023\)](#), who studied *Cryptocarya alba* and
400 *Beilschmiedia miersii* (both from the Lauraceae family) that live in sclerophyllous forests in Chile, found
401 that the trees’ overall growth had slowed down. This could mean that the natural dynamics of their forests
402 have changed. They attributed it to the cumulative effects of the unprecedented drought (i.e., hydrological
403 drought). Thus, we attribute that forest to being the most resistant to drought, due to the fact that most
404 of the species comprising it are highly resilient to water scarcity compared to the other land cover classes.
405 Nonetheless, if we want to go deep in our analysis, we should use earth observation data that is able to
406 capture a higher level of detail. For example, when we used MOD13A3 with a 1km spatial resolution to
407 measure vegetation condition, it took the average condition of 1 square kilometer. Then, to use remote
408 sensing to look at how a certain type of forest (like sclerophyllous forest) changes in response to drought on
409 a local level, we should use operational products with higher spatial resolutions, like those from Landsat or
410 Sentinel. This will let us do a more thorough analysis.

411 *6.3. Soil moisture, vegetation productivity, and agricultural drought.*

412 The main external factors that affect biomass production by vegetation are actual evapotranspiration and
413 soil moisture, and the rate of ET in turn depends on the availability of water storage in the root zone.

414 Thus, soil moisture plays a key role in land carbon uptake and, consequently, in the production of biomass
415 (Humphrey et al., 2021). Moreover, Zhang et al. (2022) indicate there is a bidirectional causality between
416 soil moisture and vegetation productivity. Lastly, some studies have redefined agricultural drought as soil
417 moisture drought from a hydrological perspective (Van Loon et al., 2016; Samaniego et al., 2018). Even
418 though soil moisture is the external factor most determinant of vegetation biomass, there are multiple internal
419 factors, such as species, physiological characteristics, and plant hydraulics, that would affect vegetation
420 productivity. Because of that, we believe that agricultural drought, referring to the drought that impacts
421 vegetation productivity, is the most proper term, as originally defined by Wilhite and Glantz (1985).

422 The study results showed that the soil moisture-based drought index (SSI) was better at explaining vegeta-
423 tion productivity across land cover macroclasses than meteorological drought indices like SPI, SPEI, and
424 EDDI. In the early growing season and especially in irrigated rather than rainfed croplands, soil moisture
425 has better skills than SPI and SPEI for estimating gross primary production (GPP). This according to
426 Chatterjee et al. (2022) evaluation of the SPI and SPEI and their correlation with GPP in the CONUS.
427 Also, Zhou et al. (2021) indicate that the monthly scaled Standardized Water Deficit Index (SWDI) can
428 accurately show the effects of agricultural drought in most of China. Nicolai-Shaw et al. (2017) also looked
429 at the time-lag between the SWDI and the Vegetation Condition Index (VCI). They found that there was
430 little to no time-lag in croplands but a greater time-lag in forests.

431 In our case, there is strong spatial variability throughout Chile and between classes, mainly attributable to
432 climate heterogeneity, hydrological status, or vegetation resistance to water scarcity. The semi-arid “Norte
433 Chico” and the Mediterranean “Centro” were where SSI had the best performance. In Chile, medium-term
434 deficits of 12 months are more relevant in the response of vegetation, which decreases to the south, and in the
435 case of croplands, they seem to react in a shorter time, with six months (SSI-6) in “Centro.” This variation
436 for croplands could be related to the fact that in “Norte Chico,” the majority of crops are irrigated, but
437 to the south there is a higher proportion of rainfed agriculture, which is most dependent on the short-term
438 availability of water. Rather, in the “Norte Chico,” the orchards are more dependent on the storage of water
439 in dams of groundwater reservoirs, which are affected by long-term drought (e.g., SPI-36).

440 6.4. Future outlook (to complete)

441 7. Conclusion

442 There is a trend toward decreasing water supply in most parts of Chile, particularly in the “Centro” and
443 “Norte Chico” regions. The whole country showed an increase in AED. Vegetation productivity only showed
444 a decrease in the “Norte Chico” and “Centro,” being highest for shrubland and croplands. Forest is the land
445 cover most resistant to drought, as shown along Chile, and shrubland and cropland are the most sensitive.

446 A soil moisture deficit of 12 months (SSI-12) is highly correlated with vegetation productivity for the land
447 cover classes of shrubland, savannas, croplands, and forest in “Norte Chico” and “Centro.” For the southern
448 part of the country with humid conditions, the correlation with SSI decreases. Soil moisture overcomes
449 the capacity to explain vegetation productivity over the supply and demand drought indices in the entire
450 territory.

451 The variation in vegetation productivity appears to be associated with climate variation rather than an-
452 thropogenic factors (e.g., an increase in water demand by irrigated crops). Even though switching to more
453 demanding crops on the land could increase the impact of drought on vegetation, this would need to be
454 more thoroughly investigated, for instance at the watershed level.

455 The results of this study could help in the development of a robust forecasting system for land cover classes
456 in Chile, helping to improve preparedness for climate change impacts on vegetation.

457 **Supplementary material**

458 **References**

- 459 Abramowitz, M., Stegun, I.A., 1968. Handbook of mathematical functions with formulas, graphs, and mathematical tables. 460 volume 55. US Government printing office.
- 461 Aceituno, P., Boisier, J.P., Garreaud, R., Rondanelli, R., Rutllant, J.A., 2021. Climate and Weather in Chile, in: Fernández, 462 B., Gironás, J. (Eds.), Water Resources of Chile. Springer International Publishing, Cham. volume 8, pp. 7–29. URL: 463 http://link.springer.com/10.1007/978-3-030-56901-3_2.
- 464 AghaKouchak, A., Mirchi, A., Madani, K., Di Baldassarre, G., Nazemi, A., Alborzi, A., Anjileli, H., Azarderakhsh, M., Chiang, 465 F., Hassanzadeh, E., Huning, L.S., Mallakpour, I., Martinez, A., Mazdiyasni, O., Moftakhari, H., Norouzi, H., Sadegh, 466 M., Sadeqi, D., Van Loon, A.F., Wanders, N., 2021. Anthropogenic Drought: Definition, Challenges, and Opportunities. 467 Reviews of Geophysics 59, e2019RG000683. URL: <https://agupubs.onlinelibrary.wiley.com/doi/10.1029/2019RG000683>, doi:[10.1029/2019RG000683](https://doi.org/10.1029/2019RG000683).
- 468 Akinyemi, F.O., 2021. Vegetation Trends, Drought Severity and Land Use-Land Cover Change during the Growing Season in 469 Semi-Arid Contexts. Remote Sensing 2021, Vol. 13, Page 836 13, 836. URL: <https://www.mdpi.com/2072-4292/13/5/836/> htm, doi:[10.3390/RS13050836](https://doi.org/10.3390/RS13050836). publisher: Multidisciplinary Digital Publishing Institute.
- 470 Bakker, K., 2012. Water Security: Research Challenges and Opportunities. Science 337, 914–915. URL: <https://www.science.org/doi/10.1126/science.1226337>, doi:[10.1126/science.1226337](https://doi.org/10.1126/science.1226337).
- 471 Beck, H.E., McVicar, T.R., Vergopolan, N., Berg, A., Lutsko, N.J., Dufour, A., Zeng, Z., Jiang, X., van Dijk, A.I.J.M., Miralles, 472 D.G., 2023. High-resolution (1 km) Köppen-Geiger maps for 1901–2099 based on constrained CMIP6 projections. Scientific 473 Data 10. URL: <http://dx.doi.org/10.1038/s41597-023-02549-6>, doi:[10.1038/s41597-023-02549-6](https://doi.org/10.1038/s41597-023-02549-6).
- 474 Beguería, S., Vicente-Serrano, S.M., 2023. SPEI: Calculation of the Standardized Precipitation-Evapotranspiration Index. 475 URL: <https://CRAN.R-project.org/package=SPEI>.
- 476 Boisier, J.P., Alvarez-Garreton, C., Cordero, R.R., Damiani, A., Gallardo, L., Garreaud, R.D., Lambert, F., Ramallo, C., 477 Rojas, M., Rondanelli, R., 2018. Anthropogenic drying in central-southern Chile evidenced by long-term observations 478 and climate model simulations. Elementa 6, 74. URL: <https://www.elementascience.org/article/10.1525/elementa.328/>, doi:[10.1525/elementa.328](https://doi.org/10.1525/elementa.328).
- 479 Calvin, K., Dasgupta, D., Krinner, G., Mukherji, A., Thorne, P.W., Trisos, C., Romero, J., Aldunce, P., Barrett, K., Blanco, 480 G., Cheung, W.W., Connors, S., Denton, F., Diongue-Niang, A., Dodman, D., Garschagen, M., Geden, O., Hayward, B., 481 Jones, C., Jotzo, F., Krug, T., Lasco, R., Lee, Y.Y., Masson-Delmotte, V., Meinshausen, M., Mintenbeck, K., Mokssit, A., 482 Otto, F.E., Pathak, M., Pirani, A., Poloczanska, E., Pörtner, H.O., Revi, A., Roberts, D.C., Roy, J., Ruane, A.C., Skea, 483 J., Shukla, P.R., Slade, R., Slangen, A., Sokona, Y., Sörensson, A.A., Tignor, M., Van Vuuren, D., Wei, Y.M., Winkler, 484 H., Zhai, P., Zommers, Z., Hourcade, J.C., Johnson, F.X., Pachauri, S., Simpson, N.P., Singh, C., Thomas, A., Totin, E., 485 Arias, P., Bustamante, M., Elgizouli, I., Flato, G., Howden, M., Méndez-Vallejo, C., Pereira, J.J., Pichs-Madruga, R., Rose, 486 S.K., Saheb, Y., Sánchez Rodríguez, R., Ürge Vorsatz, D., Xiao, C., Yassa, N., Alegría, A., Armour, K., Bednar-Friedl, B., 487 Blok, K., Cissé, G., Dentener, F., Eriksen, S., Fischer, E., Garner, G., Guiavarch, C., Haasnoot, M., Hansen, G., Hauser, M., 488 Hawkins, E., Hermans, T., Kopp, R., Leprince-Ringuet, N., Lewis, J., Ley, D., Ludden, C., Niamir, L., Nicholls, Z., Some, 489 S., Szopa, S., Trewin, B., Van Der Wijst, K.I., Winter, G., Witting, M., Birt, A., Ha, M., Romero, J., Kim, J., Haites, E.F., 490 Jung, Y., Stavins, R., Birt, A., Ha, M., Orendain, D.J.A., Ignon, L., Park, S., Park, Y., Reisinger, A., Cammaramo, D., 491 Fischlin, A., Fuglestvedt, J.S., Hansen, G., Ludden, C., Masson-Delmotte, V., Matthews, J.R., Mintenbeck, K., Pirani, A., 492 Poloczanska, E., Leprince-Ringuet, N., Péan, C., 2023. IPCC, 2023: Climate Change 2023: Synthesis Report. Contribution 493 of Working Groups I, II and III to the Sixth Assessment Report of the Intergovernmental Panel on Climate Change [Core 494 Writing Team, H. Lee and J. Romero (eds.)]. IPCC, Geneva, Switzerland. Technical Report. Intergovernmental Panel on 495 Climate Change (IPCC). URL: <https://www.ipcc.ch/report/ar6/syr/>.
- 496 Chamling, M., Bera, B., 2020. Spatio-temporal Patterns of Land Use/Land Cover Change in the Bhutan–Bengal Foothill Region 497 Between 1987 and 2019: Study Towards Geospatial Applications and Policy Making. Earth Systems and Environment 4, 498 117–130. URL: <http://link.springer.com/10.1007/s41748-020-00150-0>, doi:[10.1007/s41748-020-00150-0](https://doi.org/10.1007/s41748-020-00150-0).
- 499 Chatterjee, S., Desai, A.R., Zhu, J., Townsend, P.A., Huang, J., 2022. Soil moisture as an essential component for delineating 500 and forecasting agricultural rather than meteorological drought. Remote Sensing of Environment 269, 112833. URL: 501 <https://linkinghub.elsevier.com/retrieve/pii/S0034425721005538>, doi:[10.1016/j.rse.2021.112833](https://doi.org/10.1016/j.rse.2021.112833).
- 502 Chen, J., Shao, Z., Huang, X., Zhuang, Q., Dang, C., Cai, B., Zheng, X., Ding, Q., 2022. Assessing the impact of drought- 503 land cover change on global vegetation greenness and productivity. Science of The Total Environment 852, 158499. URL: 504 <https://linkinghub.elsevier.com/retrieve/pii/S004896972205598X>, doi:[10.1016/j.scitotenv.2022.158499](https://doi.org/10.1016/j.scitotenv.2022.158499).
- 505 Crausbay, S.D., Ramirez, A.R., Carter, S.L., Cross, M.S., Hall, K.R., Bathke, D.J., Betancourt, J.L., Colt, S., Cravens, A.E., 506 Dalton, M.S., Dunham, J.B., Hay, L.E., Hayes, M.J., McEvoy, J., McNutt, C.A., Moritz, M.A., Nislow, K.H., Raheem, N., 507 Sanford, T., 2017. Defining Ecological Drought for the Twenty-First Century. Bulletin of the American Meteorological Society 508 98, 2543–2550. URL: <https://journals.ametsoc.org/view/journals/bams/98/12/bams-d-16-0292.1.xml>, doi:[10.1175/BAMS-D-16-0292.1](https://doi.org/10.1175/BAMS-D-16-0292.1). publisher: American Meteorological Society.
- 509 Dai, M., Huang, S., Huang, Q., Leng, G., Guo, Y., Wang, L., Fang, W., Li, P., Zheng, X., 2020. Assessing agricultural drought 510 risk and its dynamic evolution characteristics. Agricultural Water Management 231, 106003. URL: <https://linkinghub.elsevier.com/retrieve/pii/S0378377419316531>, doi:[10.1016/j.agwat.2020.106003](https://doi.org/10.1016/j.agwat.2020.106003).
- 511 Didan, K., 2015. MOD13Q1 MODIS/Terra Vegetation Indices 16-Day L3 Global 250m SIN Grid V006. Technical Report. 512 NASA EOSDIS Land Processes DAAC. doi:[http://dx.doi.org/10.5067/MODIS/MOD13Q1.006](https://dx.doi.org/10.5067/MODIS/MOD13Q1.006).
- 513

- 519 Farahmand, A., AghaKouchak, A., 2015. A generalized framework for deriving nonparametric standardized drought indicators.
 520 Advances in Water Resources 76, 140–145. URL: <https://linkinghub.elsevier.com/retrieve/pii/S0309170814002322>, doi:[10.1016/j.advwatres.2014.11.012](https://doi.org/10.1016/j.advwatres.2014.11.012).
- 521 Fathi-Taperasht, A., Shafizadeh-Moghadam, H., Minaei, M., Xu, T., 2022. Influence of drought duration and severity on
 523 drought recovery period for different land cover types: evaluation using MODIS-based indices. Ecological Indicators 141,
 524 109146. URL: <https://linkinghub.elsevier.com/retrieve/pii/S1470160X22006185>, doi:[10.1016/j.ecolind.2022.109146](https://doi.org/10.1016/j.ecolind.2022.109146).
- 525 Friedl, M., Sulla-Menashe, D., 2019. MCD12Q1 MODIS/Terra+Aqua Land Cover Type Yearly L3 Global 500m SIN Grid V006
 526 [Data set]. NASA EOSDIS Land Processes DAAC. doi:[10.5067/MODIS/MCD12Q1.006](https://doi.org/10.5067/MODIS/MCD12Q1.006).
- 527 Fuentes, I., Fuster, R., Avilés, D., Vervoort, W., 2021. Water scarcity in central Chile: the effect of climate and land cover
 528 changes on hydrologic resources. Hydrological Sciences Journal 66, 1028–1044. URL: <https://www.tandfonline.com/doi/full/10.1080/02626667.2021.1903475>, doi:[10.1080/02626667.2021.1903475](https://doi.org/10.1080/02626667.2021.1903475).
- 530 Garreaud, R., Alvarez-Garreton, C., Barichivich, J., Boisier, J.P., Christie, D., Galleguillos, M., LeQuere, C., McPhee,
 531 J., Zambrano-Bigiarini, M., 2017. The 2010–2015 mega drought in Central Chile: Impacts on regional hydroclimate and
 532 vegetation. Hydrology and Earth System Sciences Discussions 2017, 1–37. URL: <http://www.hydrol-earth-syst-sci-discuss.net/hess-2017-191/>, doi:[10.5194/hess-2017-191](https://doi.org/10.5194/hess-2017-191).
- 533 Garreaud, R.D., 2009. The Andes climate and weather. Advances in Geosciences 22, 3–11. URL: <https://adgeo.copernicus.org/articles/22/3/2009/>, doi:[10.5194/adgeo-22-3-2009](https://doi.org/10.5194/adgeo-22-3-2009).
- 534 Hargreaves, G.H., 1994. Defining and Using Reference Evapotranspiration. Journal of Irrigation and Drainage Engineering 120,
 535 1132–1139. URL: <https://ascelibrary.org/doi/10.1061/%28ASCE%290733-9437%281994%29120%3A6%281132%29>, doi:[10.1061/\(ASCE\)0733-9437\(1994\)120:6\(1132\)](https://doi.org/10.1061/(ASCE)0733-9437(1994)120:6(1132)).
- 536 Hargreaves, G.H., Samani, Z.A., 1985. Reference crop evapotranspiration from temperature. Applied engineering in agriculture
 537 1, 96–99.
- 538 Heim, R.R., 2002. A Review of Twentieth-Century Drought Indices Used in the United States. Bulletin of the American
 539 Meteorological Society 83, 1149–1166. URL: <https://journals.ametsoc.org/doi/10.1175/1520-0477-83.8.1149>, doi:[10.1175/1520-0477-83.8.1149](https://doi.org/10.1175/1520-0477-83.8.1149).
- 540 Hijmans, R.J., 2023. terra: Spatial Data Analysis. URL: <https://CRAN.R-project.org/package=terra>.
- 541 Hobbins, M.T., Wood, A., McEvoy, D.J., Huntington, J.L., Morton, C., Anderson, M., Hain, C., 2016. The Evaporative Demand
 542 Drought Index. Part I: Linking Drought Evolution to Variations in Evaporative Demand. Journal of Hydrometeorology 17,
 543 1745–1761. URL: <https://journals.ametsoc.org/doi/10.1175/JHM-D-15-0121.1>, doi:[10.1175/JHM-D-15-0121.1](https://doi.org/10.1175/JHM-D-15-0121.1).
- 544 Homer, C., Dewitz, J., Jin, S., Xian, G., Costello, C., Danielson, P., Gass, L., Funk, M., Wickham, J., Stehman, S., Auch, R.,
 545 Riitters, K., 2020. Conterminous United States land cover change patterns 2001–2016 from the 2016 National Land Cover
 546 Database. ISPRS Journal of Photogrammetry and Remote Sensing 162, 184–199. URL: <https://linkinghub.elsevier.com/retrieve/pii/S0924271620300587>, doi:[10.1016/j.isprsjprs.2020.02.019](https://doi.org/10.1016/j.isprsjprs.2020.02.019).
- 547 Hufkens, K., Stauffer, R., Campitelli, E., 2019. The ecwmfr package: an interface to ECMWF API endpoints. URL: <https://bluegreen-labs.github.io/ecwmfr/>.
- 548 Humphrey, V., Berg, A., Ciais, P., Gentine, P., Jung, M., Reichstein, M., Seneviratne, S.I., Frankenberg, C., 2021. Soil
 549 moisture–atmosphere feedback dominates land carbon uptake variability. Nature 592, 65–69. URL: <https://www.nature.com/articles/s41586-021-03325-5>, doi:[10.1038/s41586-021-03325-5](https://doi.org/10.1038/s41586-021-03325-5).
- 550 IPCC, 2013. Climate Change 2013: The Physical Science Basis. Contribution of Working Group I to the Fifth Assessment
 551 Report of the Intergovernmental Panel on Climate Change. Cambridge University Press, Cambridge, UK; New York, USA.
 552 URL: www.climatechange2013.org, doi:[10.1017/CBO9781107415324](https://doi.org/10.1017/CBO9781107415324).
- 553 Jiang, W., Wang, L., Feng, L., Zhang, M., Yao, R., 2020. Drought characteristics and its impact on changes in surface
 554 vegetation from 1981 to 2015 in the Yangtze River Basin, China. International Journal of Climatology 40, 3380–3397. URL:
 555 <https://rmets.onlinelibrary.wiley.com/doi/10.1002/joc.6403>, doi:[10.1002/joc.6403](https://doi.org/10.1002/joc.6403).
- 556 Kendall, M., 1975. Rank correlation methods (4th ed. 2d impression). Griffin.
- 557 Kogan, F., Guo, W., Yang, W., 2020. Near 40-year drought trend during 1981–2019 earth warming and food security. Geomatics,
 558 Natural Hazards and Risk 11, 469–490. URL: <https://www.tandfonline.com/doi/full/10.1080/19475705.2020.1730452>, doi:[10.1080/19475705.2020.1730452](https://doi.org/10.1080/19475705.2020.1730452).
- 559 Laimighofer, J., Laaha, G., 2022. How standard are standardized drought indices? Uncertainty components for the SPI
 560 & SPEI case. Journal of Hydrology 613, 128385. URL: <https://linkinghub.elsevier.com/retrieve/pii/S0022169422009544>, doi:[10.1016/j.jhydrol.2022.128385](https://doi.org/10.1016/j.jhydrol.2022.128385).
- 561 Li, W., Migliavacca, M., Forkel, M., Denissen, J.M.C., Reichstein, M., Yang, H., Duveiller, G., Weber, U., Orth, R., 2022.
 562 Widespread increasing vegetation sensitivity to soil moisture. Nature Communications 13, 3959. URL: <https://www.nature.com/articles/s41467-022-31667-9>, doi:[10.1038/s41467-022-31667-9](https://doi.org/10.1038/s41467-022-31667-9).
- 563 Luebert, F., Pliscott, P., 2022. The vegetation of Chile and the EcoVeg approach in the context of the International Vegetation
 564 Classification project. Vegetation Classification and Survey 3, 15–28. URL: <https://vcs.pensoft.net/article/67893/>, doi:[10.3897/VCS.67893](https://doi.org/10.3897/VCS.67893).
- 565 Luyssaert, S., Jammet, M., Stoy, P.C., Estel, S., Pongratz, J., Ceschia, E., Churkina, G., Don, A., Erb, K., Ferlicoq, M.,
 566 Gielen, B., Grünwald, T., Houghton, R.A., Klumpp, K., Knohl, A., Kolb, T., Kuemmerle, T., Laurila, T., Lohila, A.,
 567 Loustau, D., McGrath, M.J., Meyfroidt, P., Moors, E.J., Naudts, K., Novick, K., Otto, J., Pilegaard, K., Pio, C.A., Rambal,
 568 S., Rebmann, C., Ryder, J., Suyker, A.E., Varlagin, A., Wattenbach, M., Dolman, A.J., 2014. Land management and
 569 land-cover change have impacts of similar magnitude on surface temperature. Nature Climate Change 4, 389–393. URL:
 570 <https://www.nature.com/articles/nclimate2196>, doi:[10.1038/nclimate2196](https://doi.org/10.1038/nclimate2196).
- 571 Masson-Delmotte, V., P.Z.A.P.S.L.C.C.P.S.B.N.C.Y.C.L.G.M.I.G.M.H.K.L.E.L.J.B.R.M.T.K.M.T.W.O.Y.R.Y.a.B.Z.e., 2021.
 572 IPCC, 2021: Climate Change 2021: The Physical Science Basis. Contribution of Working Group I to the Sixth Assessment

- Report of the Intergovernmental Panel on Climate Change. Technical Report. URL: <https://www.ipcc.ch/>. publication Title: Cambridge University Press. In Press.
- McEvoy, D.J., Huntington, J.L., Hobbins, M.T., Wood, A., Morton, C., Anderson, M., Hain, C., 2016. The Evaporative Demand Drought Index. Part II: CONUS-Wide Assessment against Common Drought Indicators. *Journal of Hydrometeorology* 17, 1763–1779. URL: <http://journals.ametsoc.org/doi/10.1175/JHM-D-15-0122.1>, doi:[10.1175/JHM-D-15-0122.1](https://doi.org/10.1175/JHM-D-15-0122.1).
- Meroni, M., Rembold, F., Fasbender, D., Vrieling, A., 2017. Evaluation of the Standardized Precipitation Index as an early predictor of seasonal vegetation production anomalies in the Sahel. *Remote Sensing Letters* 8, 301–310. URL: <http://www.tandfonline.com/doi/abs/10.1080/2150704X.2016.1264020>, doi:[10.1080/2150704X.2016.1264020](https://doi.org/10.1080/2150704X.2016.1264020).
- Miranda, A., Lara, A., Altamirano, A., Di Bella, C., González, M.E., Julio Camarero, J., 2020. Forest browning trends in response to drought in a highly threatened mediterranean landscape of South America. *Ecological Indicators* 115, 106401. URL: <https://linkinghub.elsevier.com/retrieve/pii/S1470160X20303381>, doi:[10.1016/j.ecolind.2020.106401](https://doi.org/10.1016/j.ecolind.2020.106401).
- Miranda, A., Syphard, A.D., Berdugo, M., Carrasco, J., Gómez-González, S., Ovalle, J.F., Delpiano, C.A., Vargas, S., Squeo, F.A., Miranda, M.D., Dobbs, C., Mentler, R., Lara, A., Garreaud, R., 2023. Widespread synchronous decline of Mediterranean-type forest driven by accelerated aridity. *Nature Plants* 9, 1810–1817. URL: <https://www.nature.com/articles/s41477-023-01541-7>, doi:[10.1038/s41477-023-01541-7](https://doi.org/10.1038/s41477-023-01541-7).
- Muñoz-Sabater, J., Dutra, E., Agustí-Panareda, A., Albergel, C., Arduini, G., Balsamo, G., Boussetta, S., Choulga, M., Harrigan, S., Hersbach, H., Martens, B., Miralles, D.G., Piles, M., Rodríguez-Fernández, N.J., Zsoter, E., Buontempo, C., Thépaut, J.N., 2021. ERA5-Land: a state-of-the-art global reanalysis dataset for land applications. *Earth System Science Data* 13, 4349–4383. URL: <https://essd.copernicus.org/articles/13/4349/2021/>, doi:[10.5194/essd-13-4349-2021](https://doi.org/10.5194/essd-13-4349-2021).
- Nicolai-Shaw, N., Zscheischler, J., Hirschi, M., Gudmundsson, L., Seneviratne, S.I., 2017. A drought event composite analysis using satellite remote-sensing based soil moisture. *Remote Sensing of Environment* 203, 216–225. URL: <https://linkinghub.elsevier.com/retrieve/pii/S0034425717302729>, doi:[10.1016/j.rse.2017.06.014](https://doi.org/10.1016/j.rse.2017.06.014).
- Noguera, I., Vicente-Serrano, S.M., Domínguez-Castro, F., 2022. The Rise of Atmospheric Evaporative Demand Is Increasing Flash Droughts in Spain During the Warm Season. *Geophysical Research Letters* 49, e2021GL097703. URL: <https://agupubs.onlinelibrary.wiley.com/doi/10.1029/2021GL097703>, doi:[10.1029/2021GL097703](https://doi.org/10.1029/2021GL097703).
- Pebesma, E., 2018. Simple Features for R: Standardized Support for Spatial Vector Data. *The R Journal* 10, 439–446. URL: <https://doi.org/10.32614/RJ-2018-009>, doi:[10.32614/RJ-2018-009](https://doi.org/10.32614/RJ-2018-009).
- Pebesma, E., Bivand, R., 2023. Spatial Data Science: With applications in R. Chapman and Hall/CRC, London. URL: <https://r-spatial.org/book/>.
- Peng, D., Zhang, B., Wu, C., Huete, A.R., Gonsamo, A., Lei, L., Ponce-Campos, G.E., Liu, X., Wu, Y., 2017. Country-level net primary production distribution and response to drought and land cover change. *Science of The Total Environment* 574, 65–77. URL: <https://linkinghub.elsevier.com/retrieve/pii/S0048969716319507>, doi:[10.1016/j.scitotenv.2016.09.033](https://doi.org/10.1016/j.scitotenv.2016.09.033).
- Pitman, A.J., De Noblet-Ducoudré, N., Avila, F.B., Alexander, L.V., Boisier, J.P., Brovkin, V., Delire, C., Cruz, F., Donat, M.G., Gayler, V., Van Den Hurk, B., Reick, C., Volodko, A., 2012. Effects of land cover change on temperature and rainfall extremes in multi-model ensemble simulations. *Earth System Dynamics* 3, 213–231. URL: <https://esd.copernicus.org/articles/3/213/2012/>, doi:[10.5194/esd-3-213-2012](https://doi.org/10.5194/esd-3-213-2012).
- Potopová, V., Stepánek, P., Mozný, M., Türkott, L., Soukup, J., 2015. Performance of the standarised precipitation evapotranspiration index at various lags for agricultural drought risk assessment in the {C}zech {R}epublic. *Agricultural and Forest Meteorology* 202, 26–38.
- R Core Team, 2023. R: A Language and Environment for Statistical Computing. R Foundation for Statistical Computing, Vienna, Austria. URL: <https://www.R-project.org/>.
- Rhee, J., Im, J., Carbone, G.J., 2010. Monitoring agricultural drought for arid and humid regions using multi-sensor remote sensing data. *Remote Sensing of Environment* 114, 2875–2887. URL: <http://www.sciencedirect.com/science/article/pii/S003442571000221X>, doi:[10.1016/j.rse.2010.07.005](https://doi.org/10.1016/j.rse.2010.07.005).
- Samaniego, L., Thober, S., Kumar, R., Wanders, N., Rakovec, O., Pan, M., Zink, M., Sheffield, J., Wood, E.F., Marx, A., 2018. Anthropogenic warming exacerbates European soil moisture droughts. *Nature Climate Change* 8, 421–426. URL: <https://www.nature.com/articles/s41558-018-0138-5>, doi:[10.1038/s41558-018-0138-5](https://doi.org/10.1038/s41558-018-0138-5).
- Sen, P.K., 1968. Estimates of the Regression Coefficient Based on Kendall's Tau. *Journal of the American Statistical Association* 63, 1379–1389. URL: <http://www.tandfonline.com/doi/abs/10.1080/01621459.1968.10480934>, doi:[10.1080/01621459.1968.10480934](https://doi.org/10.1080/01621459.1968.10480934).
- Senf, C., Buras, A., Zang, C.S., Rammig, A., Seidl, R., 2020. Excess forest mortality is consistently linked to drought across Europe. *Nature Communications* 11, 6200. URL: <https://www.nature.com/articles/s41467-020-19924-1>, doi:[10.1038/s41467-020-19924-1](https://doi.org/10.1038/s41467-020-19924-1).
- Slette, I.J., Post, A.K., Awad, M., Even, T., Punzalan, A., Williams, S., Smith, M.D., Knapp, A.K., 2019. How ecologists define drought, and why we should do better. *Global Change Biology* 25, 3193–3200. URL: <https://onlinelibrary.wiley.com/doi/10.1111/gcb.14747>, doi:[10.1111/gcb.14747](https://doi.org/10.1111/gcb.14747).
- Song, X.P., Hansen, M.C., Stehman, S.V., Potapov, P.V., Tyukavina, A., Vermote, E.F., Townshend, J.R., 2018. Global land change from 1982 to 2016. *Nature* 560, 639–643. URL: <https://www.nature.com/articles/s41586-018-0411-9>, doi:[10.1038/s41586-018-0411-9](https://doi.org/10.1038/s41586-018-0411-9).
- Taucare, M., Viguier, B., Figueiroa, R., Daniele, L., 2024. The alarming state of Central Chile's groundwater resources: A paradigmatic case of a lasting overexploitation. *Science of The Total Environment* 906, 167723. URL: <https://linkinghub.elsevier.com/retrieve/pii/S0048969723063507>, doi:[10.1016/j.scitotenv.2023.167723](https://doi.org/10.1016/j.scitotenv.2023.167723).
- Tennekes, M., 2018. tmap: Thematic Maps in R. *Journal of Statistical Software* 84, 1–39. doi:[10.18637/jss.v084.i06](https://doi.org/10.18637/jss.v084.i06).
- Urrutia-Jalabert, R., González, M.E., González-Reyes, A., Lara, A., Garreaud, R., 2018. Climate variability and forest fires in central and south-central Chile. *Ecosphere* 9, e02171. URL: <https://esajournals.onlinelibrary.wiley.com/doi/10.1002/ecs2.2171>, doi:[10.1002/ecs2.2171](https://doi.org/10.1002/ecs2.2171).

- 649 2171, doi:[10.1002/ecs2.2171](https://doi.org/10.1002/ecs2.2171).
- 650 Van Loon, A.F., Gleeson, T., Clark, J., Van Dijk, A.I., Stahl, K., Hannaford, J., Di Baldassarre, G., Teuling, A.J., Tallaksen, L.M., Uijlenhoet, R., Hannah, D.M., Sheffield, J., Svoboda, M., Verbeiren, B., Wagener, T., Rangecroft, S., Wanders, N., Van Lanen, H.A., 2016. Drought in the Anthropocene. *Nature Geoscience* 9, 89–91. doi:[10.1038/ngeo2646](https://doi.org/10.1038/ngeo2646).
- 651 Venegas-González, A., Juñent, F.R., Gutiérrez, A.G., Filho, M.T., 2018. Recent radial growth decline in response to increased
652 drought conditions in the northernmost Nothofagus populations from South America. *Forest Ecology and Management* 409,
653 94–104. URL: <https://linkinghub.elsevier.com/retrieve/pii/S0378112717313993>, doi:[10.1016/j.foreco.2017.11.006](https://doi.org/10.1016/j.foreco.2017.11.006).
- 654 Venegas-González, A., Muñoz, A.A., Carpintero-Gibson, S., González-Reyes, A., Schneider, I., Gipolou-Zuñiga, T., Aguilera-Betti, I., Roig, F.A., 2023. Sclerophyllous Forest Tree Growth Under the Influence of a Historic Megadrought in the
655 Mediterranean Ecoregion of Chile. *Ecosystems* 26, 344–361. URL: <https://link.springer.com/10.1007/s10021-022-00760-x>,
656 doi:[10.1007/s10021-022-00760-x](https://doi.org/10.1007/s10021-022-00760-x).
- 657 Vicente-Serrano, S.M., Azorin-Molina, C., Sanchez-Lorenzo, A., Revuelto, J., López-Moreno, J.I., González-Hidalgo, J.C.,
658 Moran-Tejeda, E., Espejo, F., 2014. Reference evapotranspiration variability and trends in Spain, 1961–2011. *Global
659 and Planetary Change* 121, 26–40. URL: <https://linkinghub.elsevier.com/retrieve/pii/S0921818114001180>, doi:[10.1016/j.gloplacha.2014.06.005](https://doi.org/10.1016/j.gloplacha.2014.06.005).
- 660 Vicente-Serrano, S.M., Beguería, S., López-Moreno, J.I., 2010. A multiscalar drought index sensitive to global warming: The
661 standardized precipitation evapotranspiration index. *Journal of Climate* 23, 1696–1718. URL: <http://dx.doi.org/10.1175/2009JCLI2909.1>, doi:[10.1175/2009JCLI2909.1](https://doi.org/10.1175/2009JCLI2909.1).
- 662 Vicente-Serrano, S.M., Peña-Angulo, D., Beguería, S., Domínguez-Castro, F., Tomás-Burguera, M., Noguera, I., Gimeno-Sotelo, L., El Kenawy, A., 2022. Global drought trends and future projections. *Philosophical Transactions of the Royal Society A: Mathematical, Physical and Engineering Sciences* 380, 20210285. URL: <https://royalsocietypublishing.org/doi/10.1098/rsta.2021.0285>, doi:[10.1098/rsta.2021.0285](https://doi.org/10.1098/rsta.2021.0285).
- 663 Vicente-Serrano, S.M., McVicar, T.R., Miralles, D.G., Yang, Y., Tomas-Burguera, M., 2020. Unraveling the influence of
664 atmospheric evaporative demand on drought and its response to climate change. *WIREs Climate Change* 11, e632. URL:
665 <https://wires.onlinelibrary.wiley.com/doi/10.1002/wcc.632>, doi:[10.1002/wcc.632](https://doi.org/10.1002/wcc.632).
- 666 Wickham, H., Averick, M., Bryan, J., Chang, W., McGowan, L.D., François, R., Grolemund, G., Hayes, A., Henry, L., Hester, J., Kuhn, M., Pedersen, T.L., Miller, E., Bache, S.M., Müller, K., Ooms, J., Robinson, D., Seidel, D.P., Spinu, V., Takahashi, K., Vaughan, D., Wilke, C., Woo, K., Yutani, H., 2019. Welcome to the tidyverse. *Journal of Open Source Software* 4, 1686.
667 doi:[10.21105/joss.01686](https://doi.org/10.21105/joss.01686).
- 668 Wilhite, D.A., Glantz, M.H., 1985. Understanding: The drought phenomenon: The role of definitions. *Water International* 10,
669 111–120. URL: <http://dx.doi.org/10.1080/02508068508686328>, doi:[10.1080/02508068508686328](https://doi.org/10.1080/02508068508686328).
- 670 Wilks, D.S., 2011. Empirical distributions and exploratory data analysis. *Statistical Methods in the Atmospheric Sciences* 100.
- 671 Winkler, K., Fuchs, R., Rounsevell, M., Herold, M., 2021. Global land use changes are four times greater than previously
672 estimated. *Nature Communications* 12, 2501. URL: <https://www.nature.com/articles/s41467-021-22702-2>, doi:[10.1038/s41467-021-22702-2](https://doi.org/10.1038/s41467-021-22702-2).
- 673 Wu, C., Zhong, L., Yeh, P.J.F., Gong, Z., Lv, W., Chen, B., Zhou, J., Li, J., Wang, S., 2024. An evaluation framework
674 for quantifying vegetation loss and recovery in response to meteorological drought based on SPEI and NDVI. *Science of
675 The Total Environment* 906, 167632. URL: <https://linkinghub.elsevier.com/retrieve/pii/S0048969723062599>, doi:[10.1016/j.scitotenv.2023.167632](https://doi.org/10.1016/j.scitotenv.2023.167632).
- 676 Xiao, C., Zaehle, S., Yang, H., Wigneron, J.P., Schmullius, C., Bastos, A., 2023. Land cover and management effects on
677 ecosystem resistance to drought stress. *Earth System Dynamics* 14, 1211–1237. URL: <https://esd.copernicus.org/articles/14/1211/2023/>, doi:[10.5194/esd-14-1211-2023](https://doi.org/10.5194/esd-14-1211-2023).
- 678 Yang, J., Huang, X., 2021. The 30 m annual land cover dataset and its dynamics in China from 1990 to 2019. *Earth System
679 Science Data* 13, 3907–3925. URL: <https://essd.copernicus.org/articles/13/3907/2021/>, doi:[10.5194/essd-13-3907-2021](https://doi.org/10.5194/essd-13-3907-2021).
- 680 Zambrano, F., 2023. Four decades of satellite data for agricultural drought monitoring throughout the growing season in Central
681 Chile, in: Vijay P. Singh Deepak Jhajharia, R.M., Kumar, R. (Eds.), *Integrated Drought Management*, Two Volume Set.
682 CRC Press, p. 28.
- 683 Zambrano, F., Lillo-Saavedra, M., Verbist, K., Lagos, O., 2016. Sixteen years of agricultural drought assessment of the
684 biobío region in chile using a 250 m resolution vegetation condition index (VCI). *Remote Sensing* 8, 1–20. URL: <http://www.mdpi.com/2072-4292/8/6/530>, doi:[10.3390/rs8060530](https://doi.org/10.3390/rs8060530). publisher: Multidisciplinary Digital Publishing Institute.
- 685 Zambrano, F., Vrieling, A., Nelson, A., Meroni, M., Tadesse, T., 2018. Prediction of drought-induced reduction of agricultural
686 productivity in Chile from MODIS, rainfall estimates, and climate oscillation indices. *Remote Sensing of Environment*
687 219, 15–30. URL: <https://www.sciencedirect.com/science/article/pii/S0034425718304541>, doi:[10.1016/j.rse.2018.10.006](https://doi.org/10.1016/j.rse.2018.10.006).
688 publisher: Elsevier.
- 689 Zambrano, F., Wardlow, B., Tadesse, T., Lillo-Saavedra, M., Lagos, O., 2017. Evaluating satellite-derived long-term historical
690 precipitation datasets for drought monitoring in Chile. *Atmospheric Research* 186, 26–42. URL: <https://www.sciencedirect.com/science/article/pii/S0169809516305865>, doi:[10.1016/j.atmosres.2016.11.006](https://doi.org/10.1016/j.atmosres.2016.11.006). publisher: Elsevier.
- 691 Zhang, W., Wei, F., Horion, S., Fensholt, R., Forkel, M., Brandt, M., 2022. Global quantification of the bidirectional dependency
692 between soil moisture and vegetation productivity. *Agricultural and Forest Meteorology* 313, 108735. URL:
693 <https://linkinghub.elsevier.com/retrieve/pii/S0168192321004214>, doi:[10.1016/j.agrformet.2021.108735](https://doi.org/10.1016/j.agrformet.2021.108735).
- 694 Zhao, Y., Feng, D., Yu, L., Wang, X., Chen, Y., Bai, Y., Hernández, H.J., Galleguillos, M., Estades, C., Biging, G.S., Radke,
695 J.D., Gong, P., 2016. Detailed dynamic land cover mapping of Chile: Accuracy improvement by integrating multi-temporal
696 data. *Remote Sensing of Environment* 183, 170–185. URL: <https://linkinghub.elsevier.com/retrieve/pii/S0034425716302188>,
697 doi:[10.1016/j.rse.2016.05.016](https://doi.org/10.1016/j.rse.2016.05.016).
- 698 Zhou, K., Li, J., Zhang, T., Kang, A., 2021. The use of combined soil moisture data to characterize agricultural drought
699 700 701 702 703 704 705 706 707 708 709 710 711 712 713

714 conditions and the relationship among different drought types in China. Agricultural Water Management 243, 106479. URL:
715 <https://linkinghub.elsevier.com/retrieve/pii/S0378377420305965>, doi:10.1016/j.agwat.2020.106479.